ELSEVIER

Contents lists available at ScienceDirect

## Soil Dynamics and Earthquake Engineering

journal homepage: www.elsevier.com/locate/soildyn





# LEAP-ASIA-2019: Validation of centrifuge experiments and the generalized scaling law on liquefaction-induced lateral spreading

Tetsuo Tobita <sup>a,\*</sup>, Kyohei Ueda <sup>b</sup>, Ruben R. Vargas <sup>b</sup>, Koji Ichii <sup>c</sup>, Mitsu Okamura <sup>d</sup>, Asri Nurani Sjafruddin <sup>d</sup>, Jiro Takemura <sup>e</sup>, Lyu Hang <sup>e</sup>, Ryosuke Uzuoka <sup>b</sup>, Susumu Iai <sup>f</sup>, Jad Boksmati <sup>g</sup>, Alessandro Fusco <sup>g</sup>, Samy Torres-Garcia <sup>g</sup>, Stuart Haigh <sup>g</sup>, Gopal Madabhushi <sup>g</sup>, Majid Manzari <sup>h</sup>, Sandra Escoffier <sup>h</sup>, Zheng Li <sup>i</sup>, Dong Soo Kim <sup>j</sup>, Satish Manandhar <sup>j</sup>, Wen-Yi Hung <sup>k</sup>, Jun-Xue Huang <sup>k</sup>, Truong-Nhat-Phuong Pham <sup>k</sup>, Mourad Zeghal <sup>l</sup>, Tarek Abdoun <sup>l</sup>, Evangelia Korre <sup>l</sup>, Bruce L. Kutter <sup>m</sup>, Trevor J. Carey <sup>m</sup>, Nicholas Stone <sup>m</sup>, Yan-Guo Zhou <sup>n</sup>, Kai Liu <sup>n</sup>, Qiang Ma <sup>n</sup>

#### ARTICLE INFO

Keywords:
Centrifuge
Liquefaction
Lateral spreading
Scaling law
Round-robin

#### ABSTRACT

A round-robin centrifuge model test for an identical saturated sloping deposit with various initial conditions was conducted in the framework of liquefaction experiments and analysis project (LEAP) with 10 international institutes. To pursue two main objectives: (1) the validation of the generalized scaling law (GSL); and, (2) the development of additional experimental data that fill the gaps in the previous LEAP, each institute was assigned two tests, identical in prototype scale: a model following the generalized scaling law and a model following conventional centrifuge scaling law. The test results show a significant match in the dynamic behavior of these models, which validates the applicability of the GSL under given conditions. However, in this study, a deviation is observed when the surface ground deformation becomes larger (i.e., 250 mm). The trend surface that correlates peak amplitude of input acceleration (PGA<sub>eff</sub>), the relative density of the ground (Dr\_ $q_c$ (2.0 m)), and surface lateral displacement (U<sub>x</sub>) is updated and confirmed with new data sets.

## 1. Introduction

More than two decades ago, VELACS [1] was one of the first attempts to validate numerical modeling for ground response under liquefaction by comparing results obtained from a series of centrifuge experiments.

Afterward, significant developments in numerical modeling have been achieved in the field of geotechnical earthquake engineering with the rapid advancement of computer science and technologies. Recently, it is common to perform numerical simulations on a design phase of major facilities to check and validate the design under seismic/wind and other

E-mail address: tobita@kansai-u.ac.jp (T. Tobita).

a Department of Civil, Environmental and Applied Systems Engineering, Kansai University, 3-3-35, Yamate-cho, Suita, Osaka, 564-8680, Japan

<sup>&</sup>lt;sup>b</sup> Disaster Prevention Research Institute, Kyoto University, Gokasho Uj, 611-0011, Japan

Faculty of Societal Safety Science, Kansai University, 7-1, Hakubai-cho, Takatsuki, Osaka, 569-1098, Japan

<sup>&</sup>lt;sup>d</sup> Department of Civil and Environmental Engineering, Ehime University, 3 Bunkyo-cho, Matsuyama, 790-8577, Japan

e Department of Civil and Environmental Eng., Tokyo Institute of Technology, 2-12-1, Ookayama, Meguro-ku, Tokyo, 152-8552, Japan

f FLIP Consortium, Kyoto, Japan

g Department of Engineering, Cambridge University, UK

h Department of Civil and Environmental Engineering, George Washington University, Washington DC, USA

<sup>&</sup>lt;sup>1</sup> Department of Geotechnique Eau et Risques, IFSTTAR, Bouguenais, France

<sup>&</sup>lt;sup>5</sup> Department of Civil and Environmental Engineering, Korean Advanced Institute of Science and Technology, KAIST, Republic of Korea

<sup>&</sup>lt;sup>k</sup> Department of Civil Engineering, National Central University, Jhongli City, Taoyuan, Taiwan

 $<sup>^{</sup>m 1}$  Department of Civil and Environmental Engineering, Rensselaer Polytechnic Institute, Troy, NY, USA

<sup>&</sup>lt;sup>m</sup> Department of Civil and Environmental Engineering, University of California, Davis, USA

<sup>&</sup>lt;sup>n</sup> Department of Civil Engineering, Zhejiang University, Hangzhou, PR China

<sup>\*</sup> Corresponding author.

Table 1
Test facilities for LEAP-ASIA-2019.

Centrifuge facility institution	L*	Shaking direction	Radius (m)	Container width/length
Cambridge University, UK	1/40	Tangential	3.56	0.45
Ehime University, Japan	1/40	Parallel to axis	1.184	0.24
IFSTTAR, France	1/50	Parallel to axis	5.063	0.5
KAIST, Rep. of Korea	1/40	Parallel to axis	5	0.45
Kyoto University, Japan	1/ 44.4	Tangential	2.5	0.32
National Central University, Taiwan	1/26	Parallel to axis	2.716	0.45
Rensselaer Poly. Inst., USA	1/23	Parallel to axis	2.7	0.42
Tokyo Inst of Tech., Japan	1/ 44.4	Parallel to axis	2.15	0.33
Univ. of California, Davis, USA	1/ 43.75	Tangential	1.094	0.63
Zhejiang University, China	1/30	Parallel to axis	4.315	0.59

loading conditions. These numerical models include FLIP [2,3], LIQCA [4], PM4SAND [5], and GEOASIA [6]. Recently, discrete element method (DEM) [7], smoothed particle hydrodynamics (SPH) [8,9], and moving particle simulation method (MPS) [10], are gaining more

attention with computational advancements (i.e., larger memory space, faster CPU and GPU speed, and so on).

Despite the efforts and findings in the above-mentioned numerical methods, the development of high-precision simulations of deformations of soil/structure systems, in which the occurrence of soil liquefaction processes is involved, remains a challenge (mainly due to the complex mechanism of liquefaction and high variability associated with nature of soils), which, has become an objective to be achieved.

Liquefaction experiments and analysis project (LEAP) is an international collaboration project aimed at validating experimental and analytical methods for studying liquefaction-related phenomena [11]. Three major exercises related to the dynamic response of a saturated sloping ground were developed as part of the LEAP framework. The first major exercise, LEAP-GWU-2015 [12], involved six centrifuge facilities for developing centrifuge models with the same target characteristics (in terms of relative density and input waves) as a uniform sandy ground of 4 m deep, and 5-degree slope with Ottawa F-65 sand. Kutter et al. [13] found a strong consistency in their results and demonstrated the feasibility of an approach for a next-generation validation database.

The following LEAP exercise was LEAP-UCD-2017; its main objective was to perform sufficient experiments to characterize the median response and the uncertainty of a specific sloping deposit of sand [14]. As part of their exercise, 24 centrifuge models were developed in nine different centrifuge facilities using the same as the previous exercise, but this time using different combinations of relative density (Dr) and peak ground acceleration (PGA). Kutter et al. [15] found consistency and

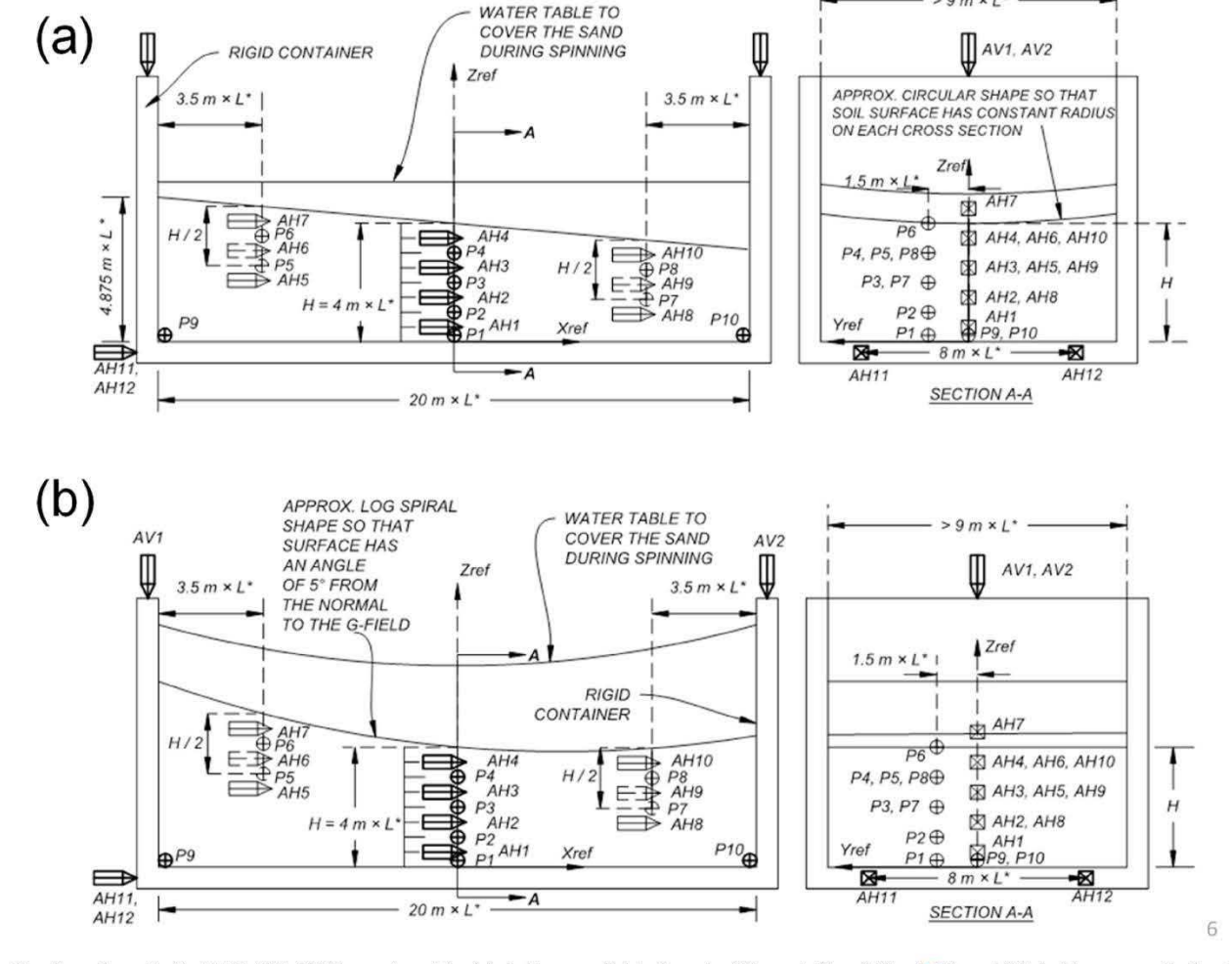


Fig. 1. Baseline schematic for LEAP-ASIA-2019 experiment for (a) shaking parallel to the axis of the centrifuge (After [13]). and (b) shaking perpendicular to the axis of the centrifuge.

 Table 2

 List of models and summary of scaling factors for each institute.

Test Type	Institute	Test ID	Test Number	Achieved Centrifuge acc	Virtual 1G, μ	Centrifuge, $\eta$
				[1]	[2]	[3]
				G		· <del></del>
A	CU	CU2 (2017)	1A	40.0	1.0	40.0
	Ehime	Ehime2 (2017)	2A	40.0	1.0	40.0
	IFSTTAR	IFSTTAR_A_A1_1	3A	50.0	1.0	50.0
	KAIST	KAIST_A_A1_1	4A	40.0	1.0	40.0
	KyU	KyU_A_A1_1	5A	44.4	1.0	44.4
	KyU	KyU_A_A2_1	6A	44.4	1.0	44.4
	NCU	NCU_A_A1_1	7A	26.0	1.0	26.0
	RPI	RPI_A_A1_1	8A	23.0	1.0	23.0
	UCD	UCD_A_A1_1	9A	43.8	1.0	43.8
	UCD	UCD_A_A2_1	10A	43.8	1.0	43.8
	ZJU	ZJU_A_A1_1	11A	30.0	1.0	30.0
	TIT	TIT_A_A1_1	12A	44.4	1.0	44.4
	TIT	TIT_A_A2_1	13A	44.4	1.0	44.4
В	CU	CU_A_B1_1	1B	71.6	0.5	80.0
	Ehime	Ehime_A_B1_1	2B	20.0	2.0	20.0
	<b>IFSTTAR</b>	IFSTTAR_A_B1_1	3B	25.0	2.0	25.0
	KAIST	KAIST_A_B1_1	4B	26.7	1.5	26.7
	KyU	KyU_A_B1_1	5B	22.2	2.0	22.2
	KyU	KyU_A_B1_2	5B	11.1	4.0	11.1
	KyU	KyU_A_B2_1	6B	22.2	2.0	22.2
	NCU	NCU_A_B1_1	7B	13.0	2.0	13.0
	RPI	RPI_A_B1_1	8A	46.0	0.5	46.0
	UCD	UCD_A_B1_1	9B	21.9	2.0	21.9
	ZJU	ZJU_A_B1_1	11B	15.0	2.0	15.0
	TIT	TIT_A_B1_1	12B	22.2	2.0	22.2
	TIT	TIT_A_B2_1	13B	22.2	2.0	22.2

M&V = Mass and Density, qc2.0 = CPT resistance at GL-2m at the median.

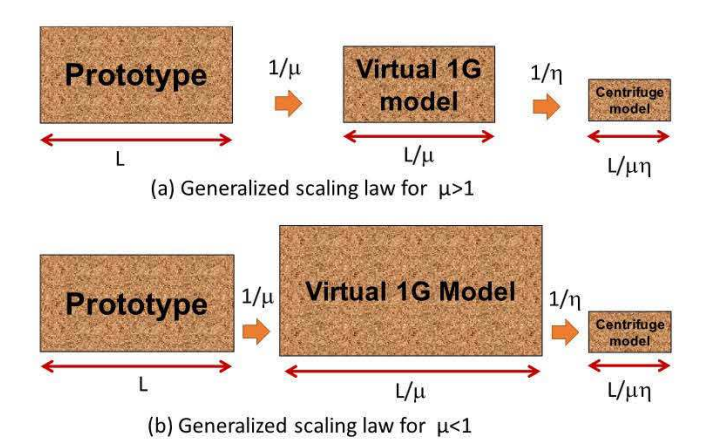


Fig. 2. Concept of the generalized scaling law for (a)  $\mu>1$  and (b)  $\mu<1.$ 

**Table 3**Scaling factors in physical model testing (Iai et al., 2005).

	(1)	(2)	(3)
	Scaling factors	Scaling factors for	Generalized scaling
	for 1-g test	centrifuge test	factors
Length	μ	η	μη
Density	1	1	1
Time	$\mu^{0.75}$	η	$\mu^{0.75}\eta$
Frequency	$\mu^{-0.75}$	1/η	$\mu^{-0.75}/\eta$
Acceleration	1	1/η	1/η
Velocity	$\mu^{0.75}$	1	μ <sup>0.75</sup>
Displacement	μ <sup>1.5</sup>	η	$\mu^{1.5}\eta$
Stress	μ	1	μ
Strain	$\mu^{0.5}$	1	$\mu^{0.5}$
Stiffness	$\mu^{0.5}$	1	u <sup>0.5</sup>
Permeability	μ <sup>0.75</sup>	η	μ <sup>0.75</sup> η
Pore pressure	μ	1	μ

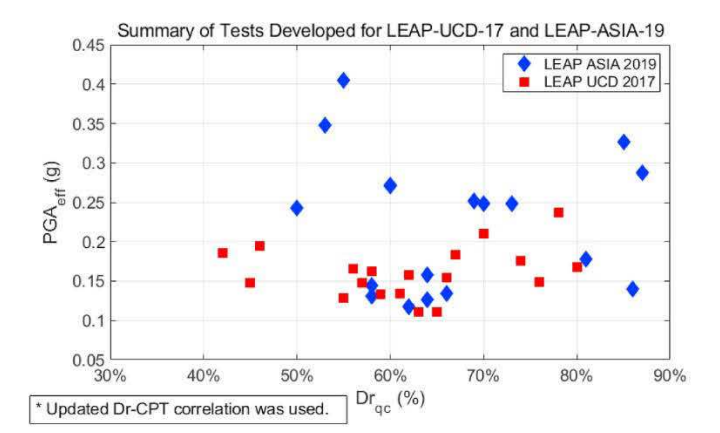


Fig. 3. Range of relative density and  $PGA_{eff}$  of the base excitation covered in LEAP-UCD-2017 and LEAP-ASIA-2019.

trends in the experiments and proposed a relationship between model ground density, PGA of input motion, and the resulting ground deformation.

Based on the success of the previous exercises, LEAP-ASIA-2019 was designed to pursue two main objectives: (1) validation of the "Generalized Scaling Law (hereafter called "GSL") [16] for centrifuge modeling; and, (2) the development of additional experimental data that fill the gaps in the data of "LEAP-UCD-2017" (in terms of combinations of Dr and PGA), to extend, establish and confirm the observed trends; in this sense, the experiments were designed to target identical geometries (in prototype scale) with the ones used in UCD-2017; hence, in ASIA-2019, the major part of model specifications were taken from Kutter et al. [14]. During ASIA-2019, ten institutes conducted 24 centrifuge tests. Specifications of the centrifuge facility of each institute, such as length scale factor, shaking direction, radius, and container width/length ratio are listed in Table 1.

**Table 4a**Summary of density measures for each of the models.

Test Type	Test ID	Test Number	Dry density from mass and volume (M&V)	Dr (M&V) assuming $\rho_max = 1757 \ \rho_min = 1491$	Pen. Resist. at 2 m depth, qc2	Density qc (2 m) = a qc^b	Dr (qc) from qc2 and $\rho$ _max = 1757 $\rho$ _min = 1491	Container Conditions	
			kg/m <sup>3</sup>	3. 5. 3.	MPa	kg/m <sup>3</sup>	AT THE	All III	
A	CU2 (2017)	1A	1606	0.47	0.95	1603	0.46	Shallow	
	Ehime2 (2017)	2A	1657	0.66	3.50	1645	0.62	Narrow	
	IFSTTAR_A_A1_1	3A	1645	0.62	1.27	1622	0.53	Shallow	
	KAIST_A_A1_1	4A	1717	0.87	5.20	1717	0.87	Shallow	
	KyU_A_A1_1	5A	1677	0.73	5.55	1667	0.70	Narrow	
	KyU_A_A2_1	6A	1628	0.56	3.61	1647	0.62	Narrow	
	NCU_A_A1_1	7A	1643	0.61	1.54	1634	0.58	Deep	
	RPI_A_A1_1	8A	1651	0.64		=		Deep	
	UCD_A_A1_1	9A	1713	0.86	3.98	1698	0.81	Shallow	
	UCD_A_A2_1	10A	1658	0.67	2.12	1656	0.66	Shallow	
	ZJU_A_A1_1	11A	1625	0.54	2.68	1640	0.60	Deep	
	TIT A A1 1	12A	1645	0.62	=	-	=	Narrow	
	TIT_A_A2_1	13A	1645	0.62	==	2-		Narrow	
В	CU_A_B1_1	1B	1606	0.47	1.10	1612	0.50	Shallow	
	Ehime A B1 1	2B	1651	0.64	4.01	1651	0.64	Narrow	
	IFSTTAR A B1 1	3B	1645	0.62	1.35	1625	0.55	Shallow	
	KAIST A B1 1	4B	1721	0.88	3.26	1684	0.76	Shallow	
	KyU A B1 1	5B	1673	0.72	5.24	1664	0.69	Narrow	
	KyU_A_B1_2	5B	1669	0.71	6.86	1677	0.73	Narrow	
	KyU_A_B2_1	6B	1633	0.58	4.03	1652	0.64	Narrow	
	NCU_A_B1_1	7B	1626	0.55	2.41	1635	0.58	Deep	
	RPI_A_B1_1	8A	1644	0.62	=	14	=	Deep	
	UCD_A_B1_1	9B	1712	0.85	5.04	1714	0.86	Shallow	
	ZJU_A_B1_1	11B	1633	0.57	2.71	1640	0.60	Deep	
	TIT_A_B1_1	12B	1654	0.65	==	-	=	Narrow	
	TIT A B2 1	13B	1648	0.63	20	F_7		Narrow	

Table 4b Summary of input motions for each of the models for the  $1^{st}$  destructive motion.

Test Type	Test ID	Test Number	Target PGA effective	Measured PGA (First Destructive Motion)	Measured PGA1 Hz (First Destructive Motion)	Estimated PGAhf (First Destructive Motion)	Estimated PGAeff (First Destructive Motion)	PGV	Arias Intensity, I <sub>a</sub>
			g	g	g	g	g	m/s	m <sup>2</sup> /s
Α	CU2 (2017)	1A	0.15	0.206	0.122	0.146	0.195	0.259	1.31
	Ehime2 (2017)	2A	0.15	0.18	0.134	0.048	0.158	0.206	1.07
	IFSTTAR_A_A1_1	3A	0.3	0.432	0.263	0.169	0.348	0.427	4.17
	KAIST_A_A1_1	4A	0.25	0.326	0.247	0.079	0.287	0.384	3.08
	KyU_A_A1_1	5A	0.25	0.304	0.191	0.113	0.248	0.278	1.89
	KyU_A_A2_1	6A	0.12	0.134	0.101	0.033	0.118	0.177	0.62
	NCU_A_A1_1	7A	0.1	0.176	0.112	0.064	0.144	0.180	0.68
	RPI_A_A1_1	8A	0.08	0.15	0.135	0.015	0.143	0.219	0.93
	UCD_A_A1_1	9A	0.2	0.213	0.143	0.07	0.178	0.271	0.93
	UCD_A_A2_1	10A	0.2	0.15	0.117	0.033	0.134	0.202	0.61
	ZJU_A_A1_1	11A	0.25	0.352	0.192	0.16	0.272	0.303	1.91
	TIT_A_A1_1	12A	0.14	0.157	0.109	0.048	0.133	0.174	0.50
	TIT_A_A2_1	13A	0.14	0.154	0.112	0.042	0.133	0.184	0.48
В	CU_A_B1_1	1B	0.15	0.326	0.159	0.167	0.243	0.224	1.49
	Ehime_A_B1_1	2B	0.18	0.198	0.117	0.081	0.158	1.998	81.26
	IFSTTAR_A_B1_1	3B	0.3	0.53	0.28	0.25	0.405	0.442	4.42
	KAIST_A_B1_1	4B	0.25	0.369	0.283	0.086	0.326	0.453	3.98
	KyU_A_B1_1	5B	0.25	0.312	0.192	0.12	0.252	0.294	1.82
	KyU_A_B1_2	5B	0.25	0.307	0.189	0.118	0.248	0.284	2.46
	KyU_A_B2_1	6B	0.12	0.163	0.089	0.074	0.126	0.155	0.78
	NCU_A_B1_1	7B	0.1	0.158	0.104	0.054	0.131	0.176	0.60
	RPI_A_B1_1	8A	0.08	0.164	0.138	0.026	0.151	0.203	0.84
	UCD_A_B1_1	9B	0.2	0.154	0.125	0.029	0.14	0.201	0.64
	ZJU_A_B1_1	11B	0.25	0.333	0.209	0.124	0.271	0.363	2.41
	TIT_A_B1_1	12B	0.14	0.145	0.099	0.046	0.122	0.168	0.57
	TIT_A_B2_1	13B	0.14	0.158	0.111	0.047	0.135	0.174	0.62

The specified model consisted of a uniform soil deposit of 4 m deep, 20 m long deposit of Ottawa F-65 sand with various dry densities, and a ground slope of  $5^{\circ}$  (Fig. 1). The target input ground motion consisted of a ramped sine wave input motion, which was similar to the target motion used in the previous exercises.

In ASIA-2019, 11 model tests with the conventional centrifuge

scaling law (hereafter called "Model A") and 13 tests with GSL (hereafter called "Model B") were conducted. All these tests are indexed as listed in Table 2. The test results in the following chapters can be identified by either "Test ID" or "Test Number." Comparable tests have the same digits in "Test Number." For example, test number "5A" of "KyU\_A\_A1\_1" of Model A is comparable with "5B" of "KyU\_A\_B1\_1" and

Table 4c Summary of surface lateral displacements for each of the models for the  $1^{st}$  destructive motion.

Test Type	Test ID	Test Number	Integrated Pos. Rel. Vel.	Peak Dynamic Rel. Disp.	Duration of liq. at P4	U <sub>x</sub> mean All Markers	U <sub>x</sub> σ All Markers	U <sub>x</sub> mean 8 Markers	U <sub>x</sub> σ 8 Markers	U <sub>x</sub> mean 2 Markers	U <sub>x</sub> σ 2 Markers
			m	m	S	mm	mm	mm	mm	mm	mm
A	CU2 (2017)	1A	5.52	0.06	28	358.9	95.7	427.5	65.0	490.0	42.4
	Ehime2 (2017)	2A	7.18	0.06	0	89.4	48.0	102.9	39.0	100.0	28.3
	IFSTTAR_A_A1_1	3A	1.33	0.09	<b>22</b>	358.3	134.5	475.0	80.2	550.0	0.0
	KAIST_A_A1_1	4A	0.51	0.04	0	30.5	13.1	34.7	9.3	33.9	0.0
	KyU_A_A1_1	5A	0.41	0.04	8	84.4	13.2	83.6	15.0	71.0	0.0
	KyU_A_A2_1	6A	0.03	0.00	0	14.5	5.6	11.1	2.4	11.1	3.1
	NCU_A_A1_1	7A	0.58	0.05	=	150.7	31.5	162.7	21.1	181.5	27.0
	RPI_A_A1_1	8A	0.45	0.04	16	87.7	22.2	0.0	0.0	99.6	13.6
	UCD_A_A1_1	9A	0.25	0.03	0	19.8	11.7	24.7	8.8	30.6	7.3
	UCD_A_A2_1	10A	0.95	0.07	8	55.6	24.4	71.8	14.2	77.5	2.6
	ZJU_A_A1_1	11A	0.93	0.08	22	321.7	100.7	393.8	32.8	390.0	42.4
	TIT_A_A1_1	12A	0.40	0.05	0	0.0	0.0	0.0	0.0	0.0	0.0
	TIT_A_A2_1	13A	0.23	0.03	0	56.2	31.2	61.1	23.0	44.4	0.0
В	CU_A_B1_1	1B	0.79	0.15	112	0.0	0.0	<u></u>		0.0	0.0
	Ehime_A_B1_1	2B	11.75	0.43	0	36.6	39.7	56.6	42.8	56.6	0.0
	IFSTTAR_A_B1_1	3B	1.16	0.08	130	555.9	178.1	685.0	108.5	777.8	100.0
	KAIST_A_B1_1	4B	0.42	0.03	0	39.6	11.1	35.6	7.1	30.6	5.4
	KyU_A_B1_1	5B	0.65	0.05	7	130.9	33.4	153.8	22.7	153.8	4.4
	KyU_A_B1_2	5B	1.13	0.06	15	111.3	25.3	116.9	26.6	115.4	12.6
	KyU_A_B2_1	6B	1.28	0.06	2	48.1	16.6	46.0	18.1	34.5	4.4
	NCU_A_B1_1	7B	0.54	0.06	0	148.7	57.6	127.8	67.9	87.2	85.9
	RPI_A_B1_1	8A	0.57	0.04	17	283.2	56.7	0.0	0.0	303.3	0.0
	UCD_A_B1_1	9B	0.98	0.07	0	-0.7	1.6	-0.7	1.9	-2.2	2.8
	ZJU_A_B1_1	11B	0.88	0.07	64	486.7	176.5	594.0	122.6	678.8	60.0
	TIT_A_B1_1	12B	0.32	0.04	0	102.0	68.3	109.9	44.4	125.6	0.0
	TIT_A_B2_1	13B	0.38	0.04	0	62.8	32.4	70.6	22.2	62.8	0.0

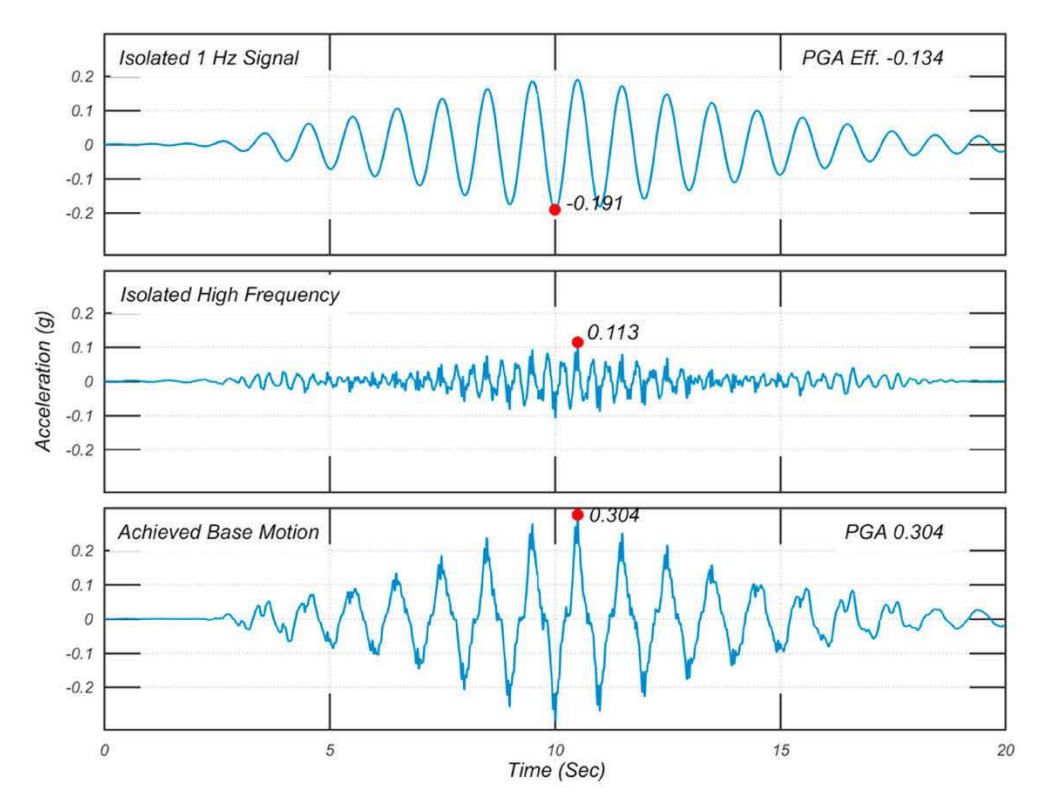


Fig. 4. Input base acceleration: Top) Isolated 1Hz signal, Mid) Isolated high frequency, and Bot) Achieved base motion (KyU\_A\_A1\_1).

"KyU\_A\_B1\_2" of Model B. There is no test number "10B," because "10A" of "UCD\_A\_A2\_1" was intended to supplement the gaps in the input parameters in the existing datasets. In this study, Model A from Cambridge University (CU) and Ehime University is taken from LEAP-UCD-2017 for comparison.

This study validates the GSL's applicability by comparing the response between Models A and B in the first destructive motion of each model test. Additional shaking or model tests must have been conducted by some institutes. These results may be reported in accompanying papers. In this study, the discussion is solely based on the results of the first

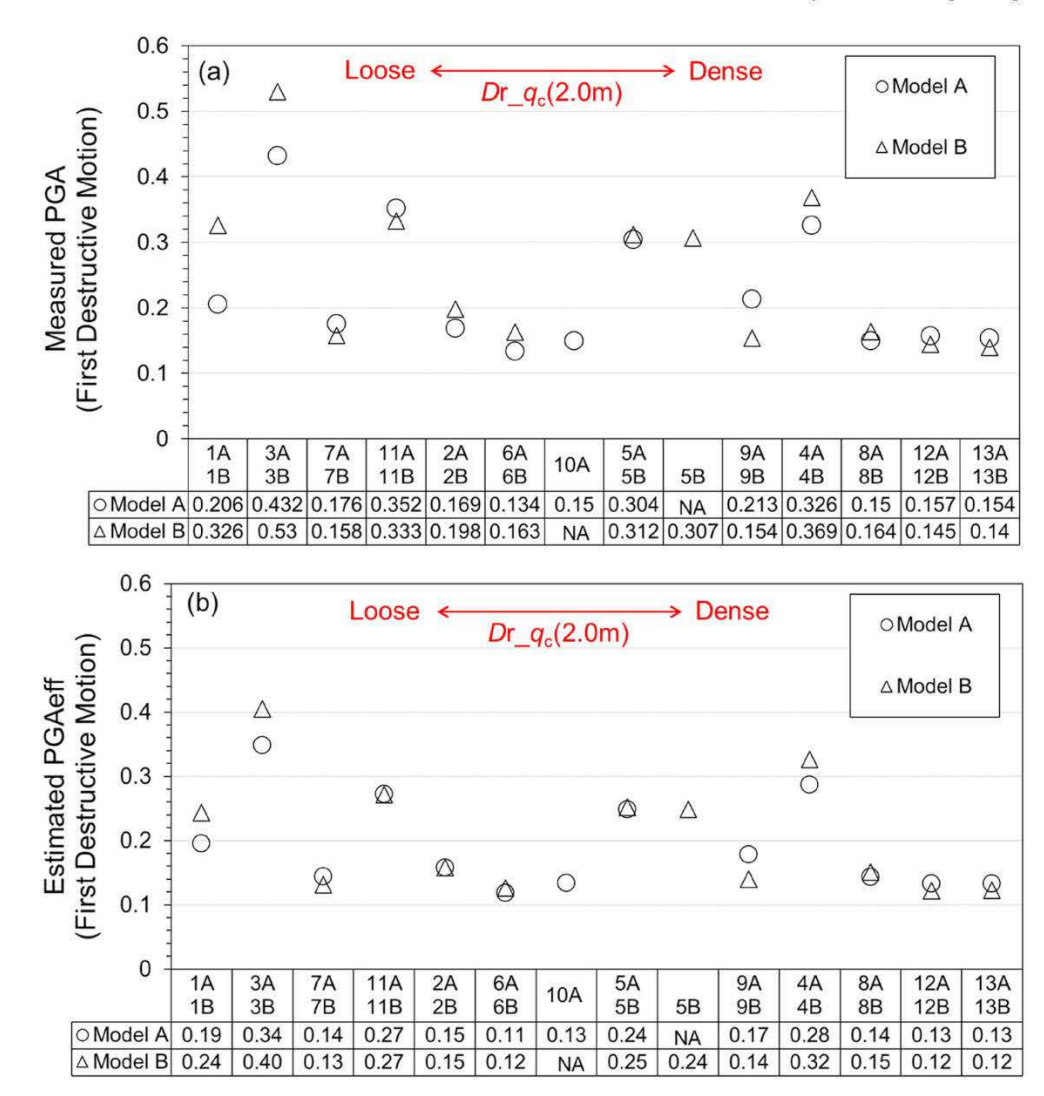


Fig. 5. Measured PGA (a) and Effective PGA<sub>eff</sub> (b) of the 1<sup>st</sup> destructive input motion sorted by the order of relative density.

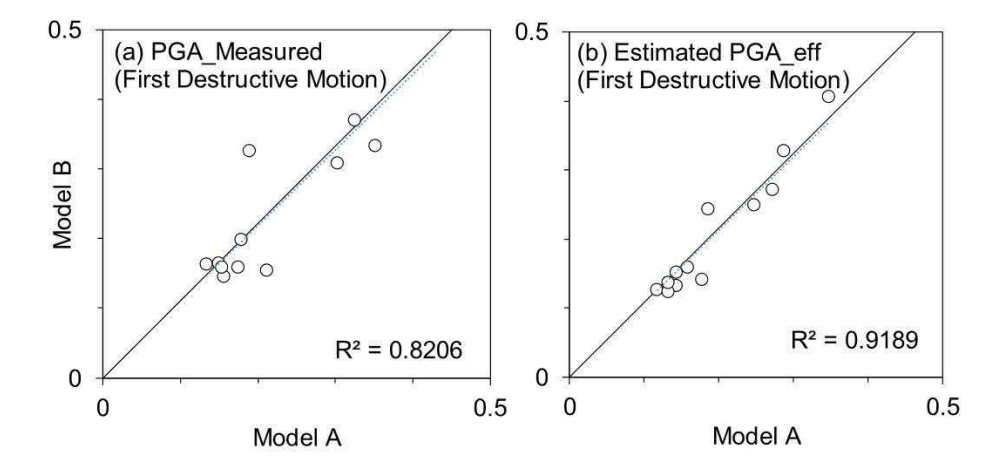


Fig. 6. Comparison of input PGA between Model A and B, (a) Measured PGA and (b) PGAeff-

destructive motion.

## 2. Generalized scaling law

In centrifuge model testing, a prototype behavior is simulated with a

scaled model that qualitatively represents its behavior. The application of physical modeling to performance-based design practice is difficult because a specific prototype cannot be tested because of testing conditions constraints, such as soil container size and scaling effects on materials. For 1-g model testing in civil engineering, larger experimental

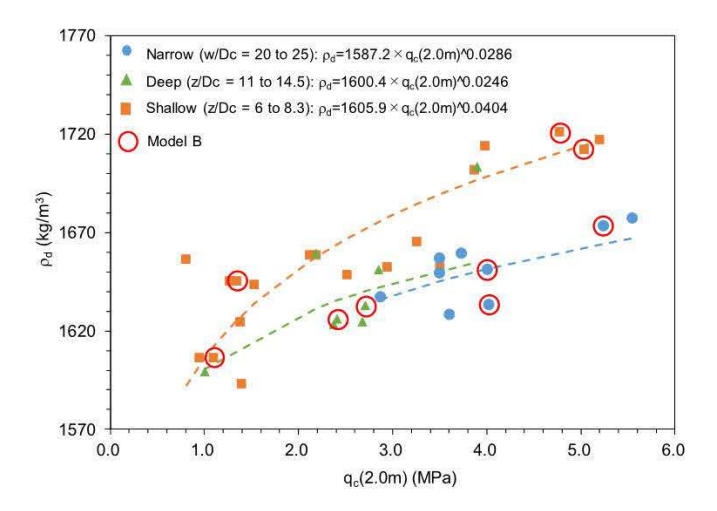


Fig. 7. Updated correlations between the dry density  $\rho_d$  and the penetration resistance  $q_c(2.0 \text{ m})$  - LEAP-UCD-2017 and LEAP-ASIA-2019(after [21]).

**Table 5** Coefficients of regression for estimated dry density,  $\rho_{\rm d}$ , through penetration resistance,  $q_{\rm c}$  (2.0 m) in each container type.

Container type		а	b
Narrow	$20 < w/D_c < 25$	1587.2	0.0286
Deep	$11 < z/D_c < 11.45$	1600.4	0.0246
Shallow	$6 < z/D_c < 8.3$	1605.9	0.0404

w: Width of container.

z: Depth of interst, i.e., z = 2 m

 $D_c$ : Diameter of a CPT rod.

a and b are coefficients of  $\rho_d = a \times q_c (2.0 \text{ m})^b$ .

facilities were built to overcome these limitations (such as E-Defense facilities, e.g. [17]); however, for geotechnical engineering, the development of large facilities still have several limitations, mainly due to the required capacity of the facilities and equipment, as well as its associated budget.

Under the aforementioned restrictions, demands for testing large prototypes are increasing. To address such demands and restrictions, Iai et al. (2005) [16] proposed a scaling law by combining the scaling law for centrifuge testing with the one for 1-g dynamic-model testing [18]. In dynamic centrifuge modeling, it was dubbed the "generalized scaling law."

The scaling factors for physical model tests are given in general forms by choosing a set of basic physical properties that are independent and deriving the scaling factors for other properties using the governing equations of the analyzed system. In the concept of the GSL, a model on a shaking table in a geotechnical centrifuge is considered as a small-scale representation of a model of a 1-g shaking-table test. This concept by introducing a "Virtual 1-g Model," in which the prototype is scaled down via a similitude for 1-g shaking-table tests, with the scaling factor of  $\mu > 1$  is visualized in Fig. 2(a). Subsequently, the virtual 1-g model is scaled down by applying a similitude for centrifuge tests to the actual physical model with the scaling factor of  $\eta > 1$ . Therefore, the geometric scaling factors used in 1-g tests ( $\mu$ ) [column (1) of Table 3] can be multiplied by those used in centrifuge tests ( $\eta$ ) [column (2) of Table 3], resulting in a much larger overall scaling factors  $\lambda = \mu \eta$  [column (3) of Table 3]

Table 2 shows the scaling factors that were used for each model. The virtual 1-g model's scaling factor ranges from 0.5 to 4.0. Here, the scaling factor of the virtual 1-g model was chosen to be less than unity,  $\mu < 1$  in two institutions, Cambridge University (CU) and Rensselaer Polytechnic Institute (RPI). The virtual 1-g model is scaled up and then scaled down to a centrifuge model, which is theoretically acceptable, but

its applicability in practice is unknown and will be tested in this study. For comparison, a larger 1-g scaling factor ( $\mu=4$ ) was used in "KyU\_A\_B1\_2."

In this study, the applicability of the GSL is examined using the modeling technique; specifically, by multiplying the overall scaling factors [column (3) of Table 3] by the physical parameters of Model B [e. g.,  $\mu=2$  (1-g scaling factor) and  $\eta=20$  (centrifuge scaling factor)], the corresponding parameters can be compared with those obtained in Model A [e.g.,  $\mu=1$  and  $\eta=40$ ].

#### 3. Model setup

As previously stated, the development of two model tests was a minimum requirement for each institute in LEAP-ASIA-2019. If any additional test was performed, and the result can be found in accompanying papers. Model A is constructed with the procedure established in LEAP-UCD-2017 (Fig. 1). On the basis of the direction of shaking against the centrifuge's axis, one of the two models shown in Fig. 1(a) (flat surface) or (b) (curved surface) was constructed. For Model B, although the model was constructed identical to Model A, the PGA of the input motion and viscosity of pore fluid were adjusted so that they become identical to the ones in Model A on the prototype scale. The two models are summarized below:

Model A: A model identical to UCD-2017 (Fig. 1) whose response can be used to fill the gaps and further extend/establish/confirm the trends obtained in UCD-2017 [15].

Model B: A model identical to Model A in prototype scale to validate the GSL (Table 3). Upon constructing the model to be tested, the input acceleration and pore fluid viscosity should be scaled to conform to the GSL.

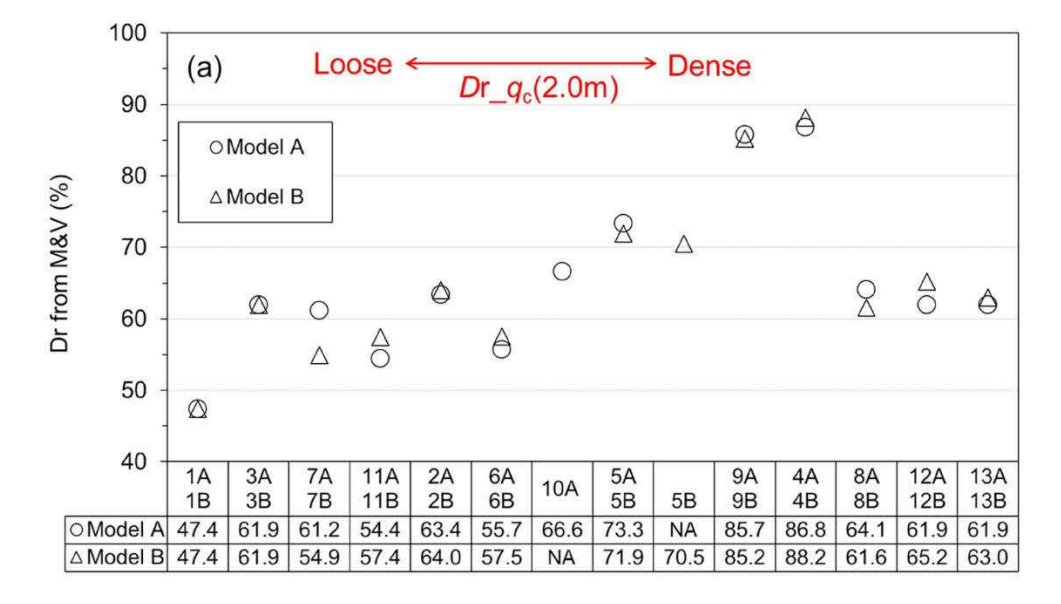
Fig. 3 compares various initial conditions, that is, PGA<sub>eff</sub> (explained in the next section) and relative density covered in the UCD-2017 and ASIA-2019 series. As previously stated, the objectives of ASIA-2019 was to fill the gaps and confirm the trends (in terms of combinations of Dr-PGA<sub>eff</sub>) of the data obtained in UCD-2017; the ASIA-2019 series have shown to cover a wider range of the relative density  $Dr_{-}q_{c}(2.0 \text{ m})$  from 47% to 85% (Table 4(a)) and the PGA<sub>eff</sub> values from 0.1 to 0.4 g (Table 4 (b)).  $Dr_{q_c}(2.0 \text{ m})$  denotes the relative density derived from the correlation with the CPT penetration resistance at 2 m depth, as discussed further below. Note that, as part of the UCD-2017, CPT test results, despite being an indirect method, are reliable in estimating the uniformity of the ground and its associated dry density compared to estimations based on mass and volume measurement [19]. As shown later, this is also confirmed in this study. Table 4(c) shows the integrated positive relative velocity [15], the surface lateral displacements derived by multiple methods for comparison and duration of liquefaction at P4 attained by each of the models.

## 3.1. Input motion and PGA<sub>eff</sub>

The target input motion consisted of a ramped 1 Hz sinusoidal wave; however, diverse additional high-frequency components were observed in the achieved motions. Note that the amount and nature of these additional high-frequency components depend mainly on the shakingtable characteristics at each facility. To standardize the PGA among the tests, and consider that higher frequency components have some but relatively small effect on the behavior of the model, the project (as a first approximation) used the concept of effective PGA, "PGA<sub>eff</sub>." The definition of PGA<sub>eff</sub> as defined by Kutter et al. [14], is shown in Equation (1); in this equation, "PGA<sub>1Hz</sub>" represents the PGA of the isolated 1 Hz component of the achieved motion, and "PGA<sub>hf</sub>" represents the higher frequency components of the ground motion.

$$PGA_{eff} = PGA_{1Hz} + 0.5*PGA_{hf}$$
 (1)

Fig. 4 shows the isolated 1 Hz motion, isolated high-frequency



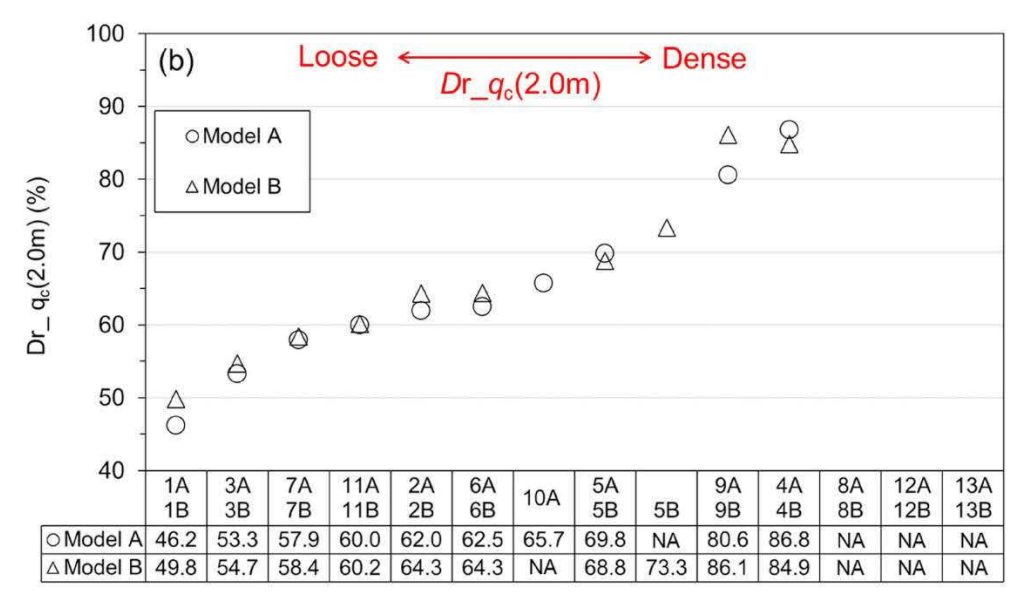


Fig. 8. Achieved relative density estimated from the CPT penetration resistance. Sorted by the order of relative density.

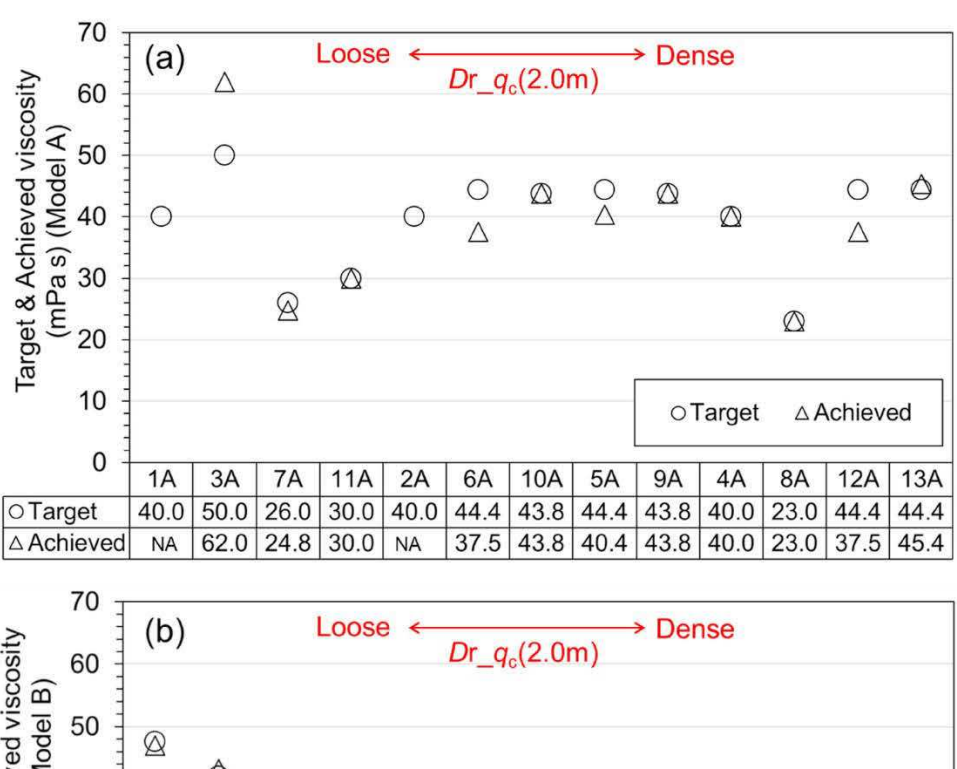
motion, and achieved base motion of the model "KyU\_A\_A1\_1."

Fig. 5 compares the measured PGA (a) and estimated PGA<sub>eff</sub> (b) of the input motion employed in each institute. The order of the institute is sorted in these figures by the relative density of the model, as indicated. These figures show that for CU and IFSTTAR with lower density and higher input PGA, severer testing conditions were assigned. Comparing Fig. 5(a) and (b), PGA<sub>eff</sub> shown in Fig. 5(b) tend to have smaller gaps between Model A and B. Fig. 6 shows that another view of the PGA comparison between Model A and B, indicates that estimated PGA<sub>eff</sub> shows better agreement between Models A and B with higher determination coefficient value ( $R^2 = 0.92$ ). From this observation, input motions of Models A and B for each institute are judged to be nearly identical on a prototype scale.

## 3.2. Dry density of the ground and $Dr_q(2.0 \text{ m})$

Kutter et al. [12] found that the penetration resistance at the mid-depth (i.e., at 2.0 m) is well correlated with the initial relative density of the ground; thus, Carey et al. used this parameter,  $q_c(2.0 \text{ m})$  [19] to linearly correlate it with the dry density based on UCD-2017

results. As Bolton et al. [20] and Kutter et al. [15] mentioned, the correlation equation is updated in this study because the  $q_c(2.0 \text{ m})$  value seems to be highly influenced by the boundary conditions (especially the container width "w" in prototype scale), and the CPT's rod diameter "Dc" in prototype scale; correlation equations depending on the size of the container or model is derived: narrow containers (w/Dc = 20-25), small models (z/Dc = 6.7-8.3), and large models (z/Dc = 11-14.5), where z is the depth measured at  $q_c(2.0 \text{ m})$ , that is, z = 2.0 m [19]. The updated chart for the relationship between dry density,  $\rho_d$  (computed from mass and volume, Table 4(a)) and tip resistance,  $q_c(2.0 \text{ m})$  is shown in Fig. 7 [after 21]. As a general trend, it is rational to observe in Fig. 7 that dry density,  $\rho_d$ , tends to increase with increasing tip resistance,  $q_c(2.0 \text{ m})$ . The results of Model B are indicated with a circle in Fig. 7, and they seem to be fitted with the trend of Model A. However, as distinguished by the color and shape of markers, the trend shows a dependence on the container types and model size. Therefore, by separating these conditions, the correlation equation is updated by including the new results of the ASIA-2019. It was found that a nonlinear regression in the form shown in Equation (2) fits better with the achieved results [21].



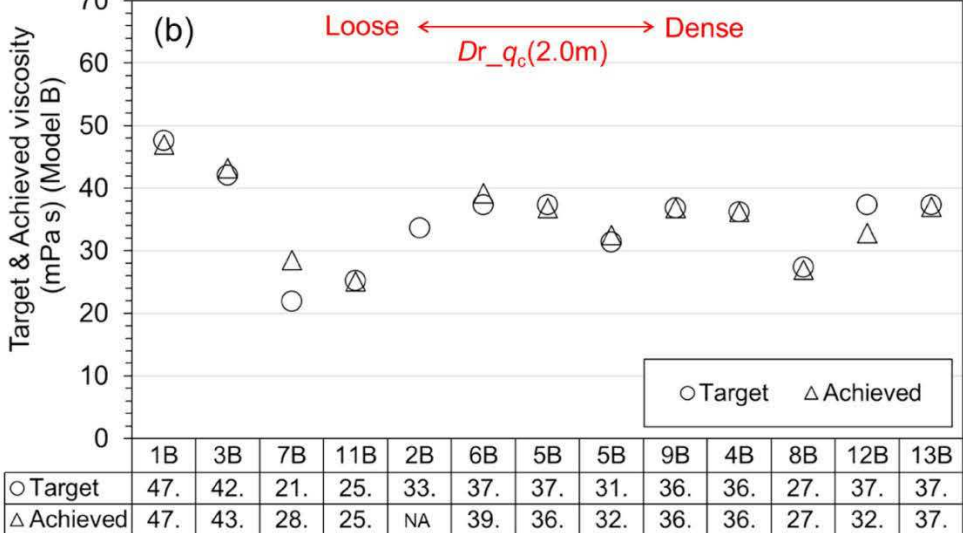


Fig. 9. Achieved viscosity of pore fluid: (a) Model A and (b) Model B. Sorted by the order of relative density.

$$\rho_d = a \times q_c(2.0m)^b \left( kg / m^3 \right) \tag{2}$$

where the unit of  $q_c(2.0 \text{ m})$  is "MPa." Table 5 lists regression parameters of a and b. Note that the achieved relative density, denoted as "Dr $_{-}q_c(2.0 \text{ m})$ ," was obtained using the above-updated correlation with the parameters  $\rho_{d_{-}{\rm max}}=1757 \, ({\rm kg/m}^3)$  and  $\rho_{d_{-}{\rm min}}=1490.5 \, ({\rm kg/m}^3)$  [22]. Fig. 8 compares the relative density obtained from mass and volume measurements (Fig. 8(a)), and those from penetration resistance (Equation (2)) (Fig. 8(b)). The overall differences in relative density between Models A and B are less than 5% as shown in the figure. Based on this observation, the initial ground conditions of Models A and B for each institute are judged to be almost identical.

## 3.3. Viscosity of pore fluid

To validate the GSL, the viscosity should be properly scaled to simulate the excess pore water pressure's diffusion process. In centrifuge modeling, methylcellulose solution is commonly used [23,24]. Because the solution is known to be temperature sensitive, each institute carefully adjusted to its viscosity. Some institutes have used cup and bob viscometers to measure viscosity, whereas others used capillary viscometers or vibration type viscometers. Fig. 9 compares the target and

achieved viscosity of pore fluid for Models A (Fig. 9(a)) and Model B (Fig. 9(b)). The difference between Model A of IFSTTAR (3A) shown in Fig. 9(a) (approximately 10 mPa s) and the others, is larger because achieved viscosity had to be measured, for some reason, by taking the fluid on the ground surface, which could contain impurities. The measured viscosity of each model in Model B is close to the target.

## 4. Test results

#### 4.1. Penetration resistance

Most tests used a miniature CPT developed in UCD-2017 [14,15] to measure ground stiffness/strength. In the profiles of the obtained penetration resistance in Fig. 10, CPT1 corresponds to CPT measured before the first destructive motion, CPT2 the one after the first destructive motion (before the second destructive motion if available), and CPT3, if plotted, the one after the second destructive motion. In Model B, the penetration depth is converted by multiplying the scaling of length ( $\mu\eta$ ) to the recorded depth. Penetration resistance in prototype scale is derived from the following Eq. (3),

$$q_c = \frac{F_{cm}}{A} \times \mu \times \frac{1}{1000} \text{ (Mpa)}$$

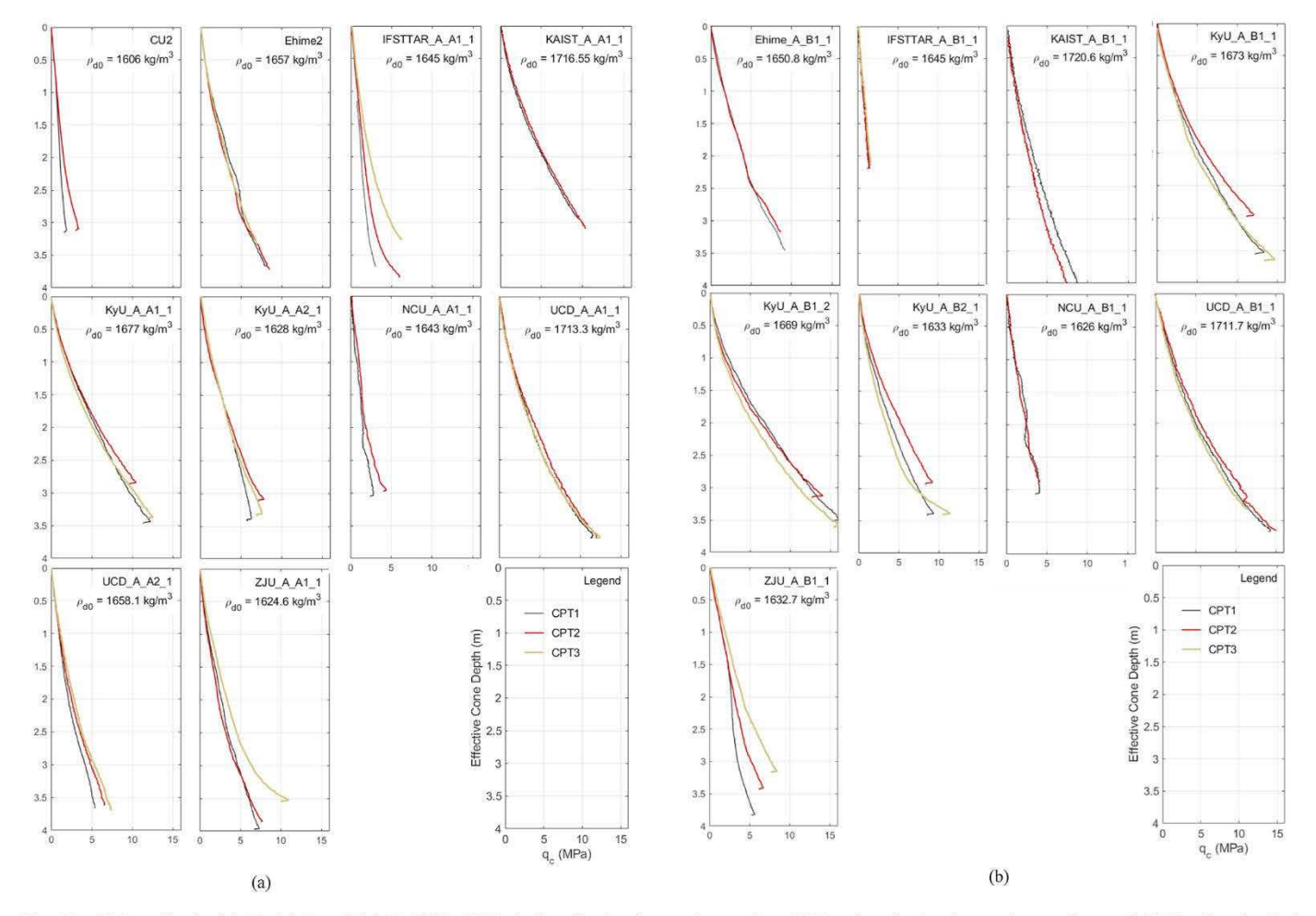


Fig. 10. CPT profile for (a) Model A and (b) Model B: CPT1: before the 1st destructive motion, CPT2: after the 1st destructive motion, and CPT3: after the 2nd destructive motion.

where  $F_{\rm cm}$  (kN) is the recorded penetration force in model scale and A (m<sup>2</sup>) is the cross-section area of the rod in model scale.

Penetration resistance of CU, IFSTTAR, NCU and ZJU show larger increments after shaking because the initial model ground was softer (Dr $_q$ c(2.0 m) < approx. 60%). CPT profiles, generally tend to increase with depth in a range of 5–15 MPa in Model A and B.

Fig. 11 compares CPT penetration resistance,  $q_c$ , of Models A and B at the depth of 1.5, 2.0, 2.5, and 3.0 m for each institute. At shallower depths, the  $q_c$  values of Models A and B agree well, but the deviation increases as they go deeper (GL 2.5 and 3.5 m). This trend is shown in Fig. 12, which provides a different view of the comparison between Model A and B. Although they agree well in Models A and B,  $q_c$  in Model B seems to be slightly overestimated for all the depths. Comparing the  $q_c$ values of "KyU\_A\_B1\_1" ( $\mu = 2$ ) with the case of "KyU\_A\_B1\_2" ( $\mu = 4$ ),  $q_c$ is overestimated when a large 1-g scaling factor is used (Fig. 11). This implies that the value of the 1-g scaling factor of stress,  $\mu$ , in Equation (3) may be slightly overestimated in the given experimental condition. In the 1-g scaling law proposed by Iai [18], the scaling factor of strain is rationally derived as  $\mu^{0.5}$  from the dependency of stiffness on confining stress (Table 3). However, the results shown in Fig. 12 enable us to improve the 1-g scaling law with accurate measurements of ground strength/stiffness as suggested by Iai [18], who proposed tuning through shear wave velocity for a more accurate estimation of the scaling factor of strain. This will be investigated elsewhere in the future.

#### 4.2. Acceleration

All acceleration records in the middle array (AH1 to AH4) and the average of two bottom accelerometers (AH11 and AH12) are plotted in Fig. 13(a) for Model A and Fig. 13(b) for Model B. Although response acceleration depends on the ground density and input motion, in most cases, dilatancy spikes with negative acceleration because of the deformation in the downstream direction appears on the records at the shallow depth. Although the sensor's polarity should be checked, depending on the overall system resonant frequency, it can be possible to have larger positive spikes in the acceleration records. The CU records show consistent positive spikes, whereas acceleration at shallow depth (AH4) of IFSTTAR shows the opposite trend. KAIST records with higher density (approx. Dr = 90%) and larger  $PGA_{eff}$  (approx. 0.3) show significant agreements between Models A and B in terms of waveforms with dilatancy spikes. On the waveforms of response acceleration of the cases with the dense ground with lower PGA<sub>eff</sub> of Model A (UCD\_A\_A1\_1: Dr = 86%,  $PGA_{eff} = 0.178$ ) and Model B (UCD\_A\_B1\_1: Dr = 85%,  $PGA_{eff} =$ 0.14), no amplitude reduction due to liquefaction is observed. Response accelerations of NCU and ZJU (soft ground with a relative density of 60% with lower to medium PGA<sub>eff</sub> of 0.13-0.27) show agreements even under highly liquefied ground. Waveforms of TIT (approx. Dr = 60%, approx. PGA<sub>eff</sub> = 0.13) also show significant agreements on both models including dilatancy spikes, although higher frequency components, induced by crossing the capacity bound of the shaker, are observed in Model B. For the cases with the scaling factor of the virtual 1-g model being  $\mu < 1$  (CU and RPI), although the number of available measurements in CU\_A\_B1\_1 is limited, overall waveforms and timing of spikes

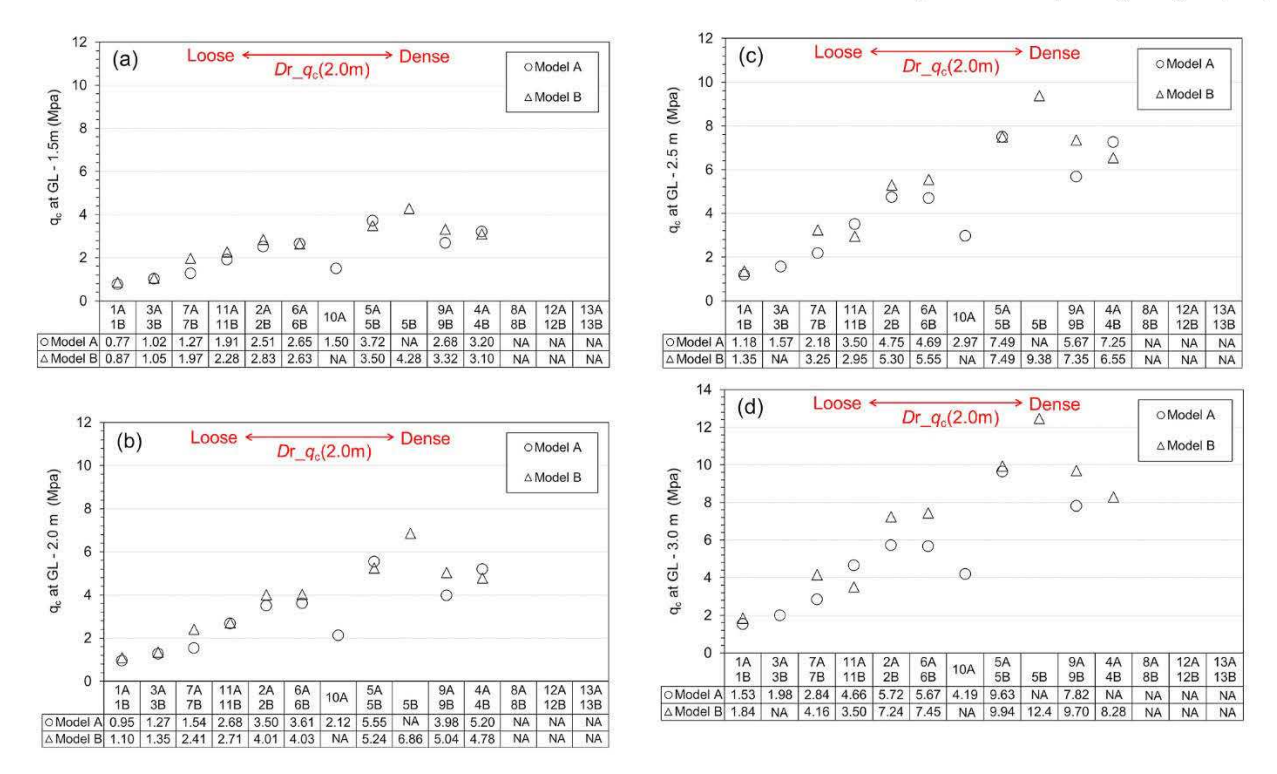


Fig. 11. CPT penetration resistance: (a) qc at 1.5 m, (b) 2.0 m, (c) 2.5 m, and (d) 3.0 m. Sorted by the order of relative density.

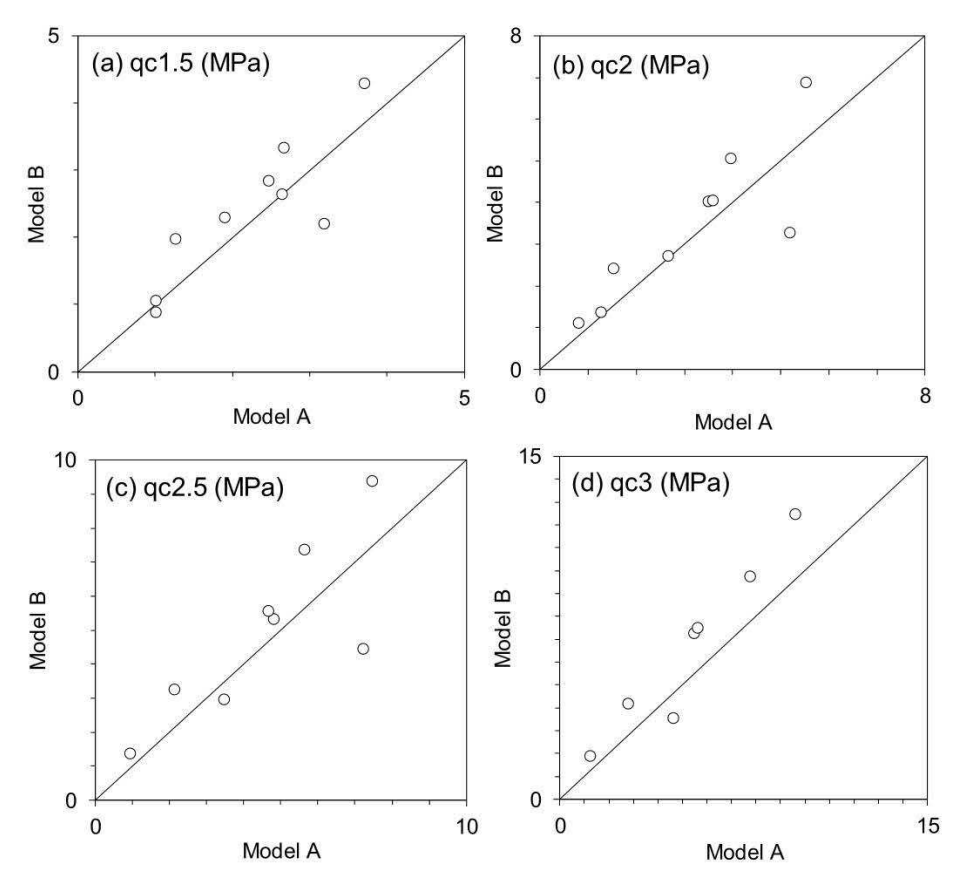


Fig. 12. Comparison of penetration resistance between Model A and B: (a)  $q_c$  at 1.5 m, (b) 2.0 m, (c) 2.5 m, and (d) 3.0 m.

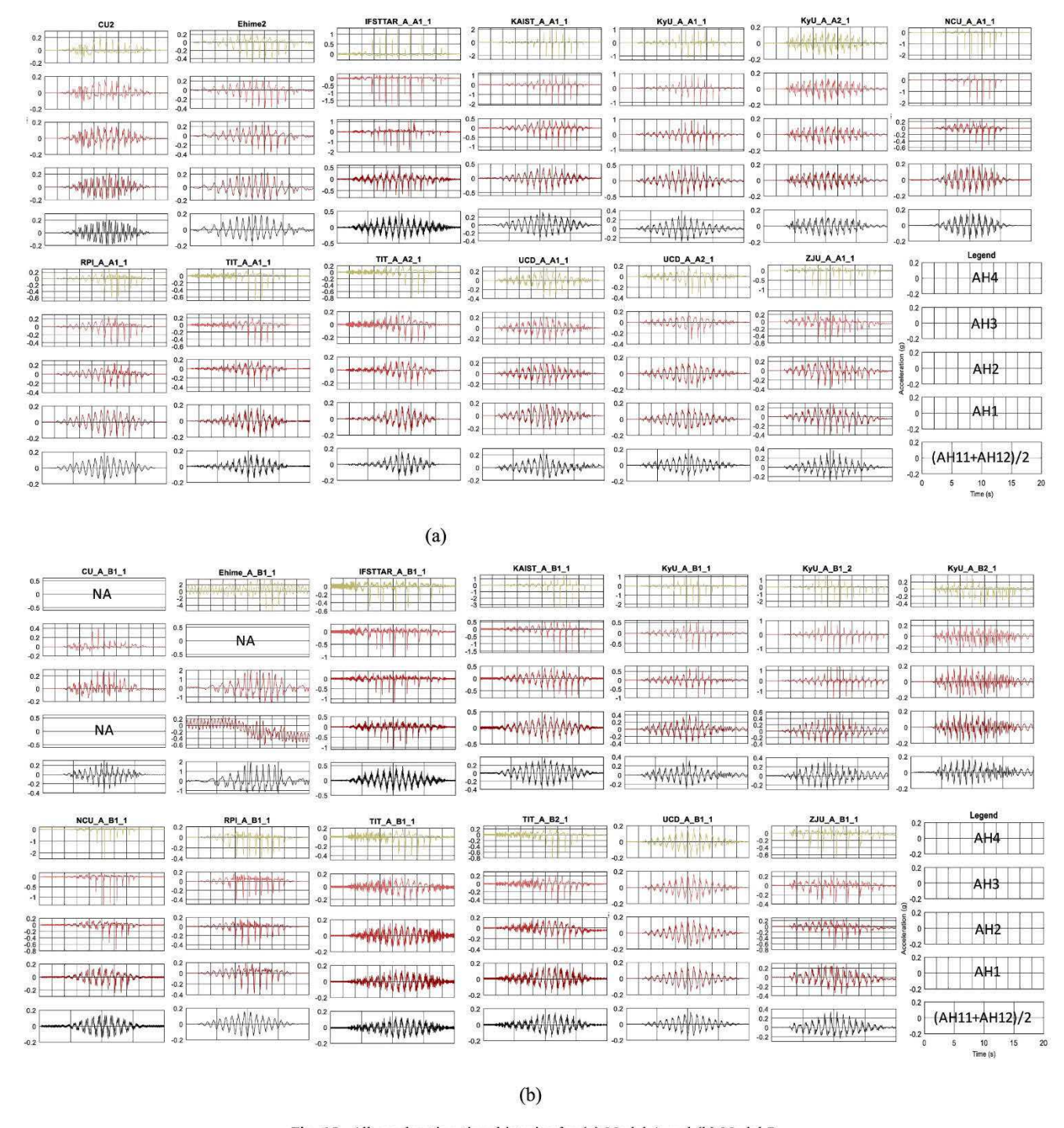


Fig. 13. All acceleration time histories for (a) Model A and (b) Model B.

are in good agreement in the records of each institute.

## 4.3. Excess pore-water pressures

Fig. 14(a) and (b) plot all the time histories of the excess pore-water pressures for Model A and B, respectively. In each figure, the time histories are separated into two parts; the first part shows the development of the excess pore pressure in the shaking phase and the latter shows the dissipation phase. Excess pore-water pressure at the bottom corner of the downstream (P10) cannot reach the initial effective stress (Fig. 14(a)). A similar trend is observed in Fig. 14(b). In Fig. 14(a) and (b), IFST-TAR\_A\_1\_1, KAIST\_A\_A1\_1, KyU\_A\_A1\_1, and ZJU\_A\_A1\_1 tend to have dilative spikes in the negative direction. Cases with the medium dense

ground with medium  $PGA_{eff}$ , such as KyU, UCD, tend to have smaller dilative spikes. For very loose ground,  $CU_A_B1_1$  shows very small spikes.

Fig. 15 compares the maximum excess pore pressure ratio of P1 to P4 between Models A and B. As shown, the maximum excess pore-water pressure is close to unity, except for CU, IFSTTAR, ZJU, and KAIST, in which lower densities and/or larger input motions might cause excessive ground deformations and high pore-water pressure. Another view of the comparison of the maximum excess pore-water pressure between Models A and B is shown in Fig. 16. Except for a few, most of the values are close to the one-to-one relationship.

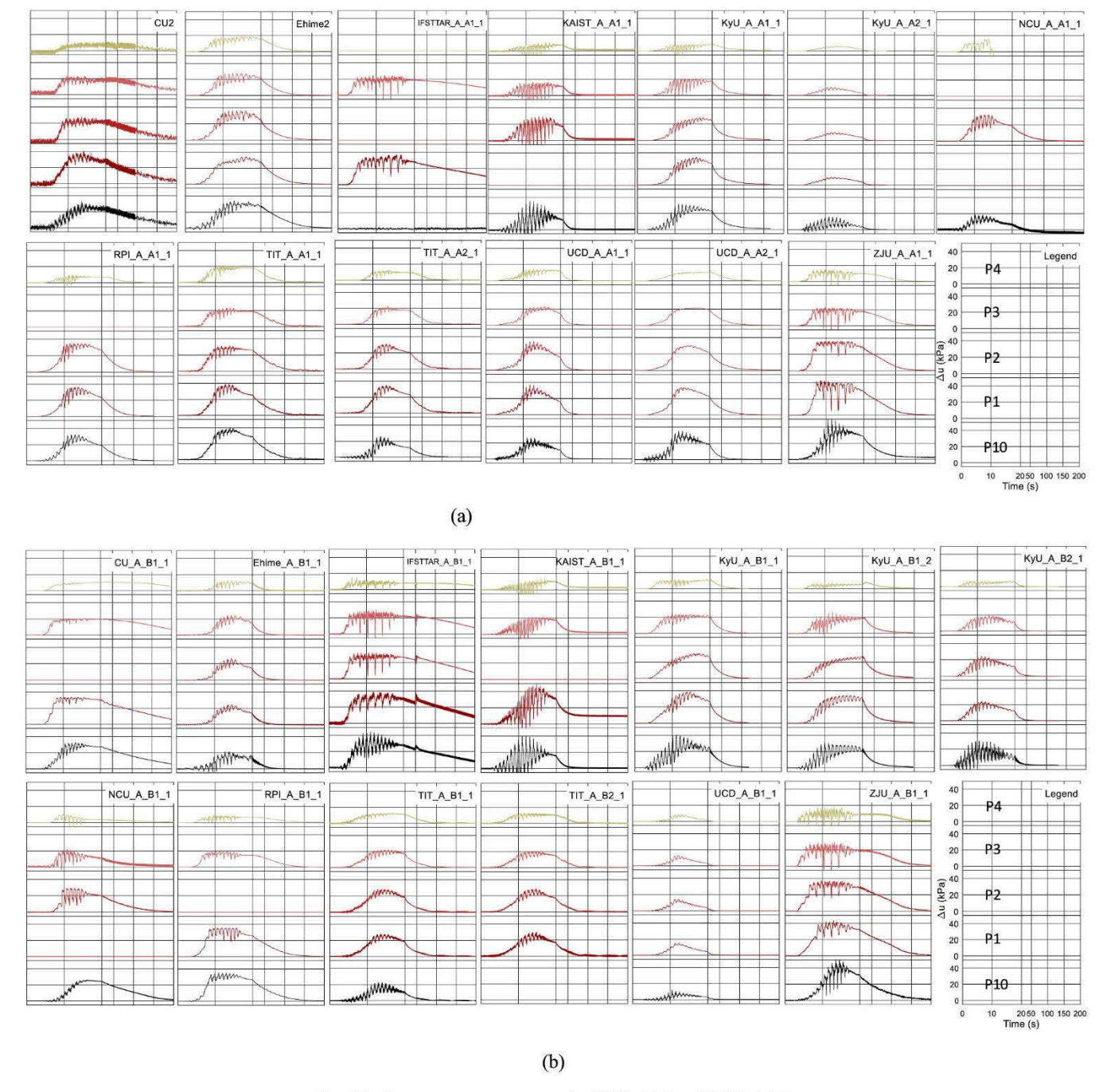


Fig. 14. Excess pore water pressure for (a) Model A and (b) Model B.

#### 4.4. Residual ground surface deformation

Residual ground surface deformation after the first destructive motion obtained by measuring the location of the surface markers are plotted with arrows in Fig. 17(a) for Model A and Fig. 17(b) for Model B. When the ground is soft (Dr\_ $q_c$ (2.0 m) < 55%) (CU, ZJU) or the PGA<sub>eff</sub> is large (PGA<sub>eff</sub> = 0.35) (IFSTTAR), lateral displacements in the downslope direction are larger (approximately 300–600 mm). However, they are necessarily uniform. Lateral displacements in the middle array are shown to be larger compared to the top (left) and bottom (right) array because of the effect of the boundary. Fig. 18 shows the lateral displacements obtained by averaging the displacement of all the markers for Model A and B. Fig. 19 compares residual displacement in the x-, y-, and z-directions. From these plots in Figs. 18 and 19, it is observed that,

when the displacements in the x-direction (downslope) are larger (i.e., more than 250 mm), in Model B, significant discrepancies in displacements between Models A and B are detected. This shows a limitation of the GSL, as implied in the scaling law of displacement,  $\mu^{1.5}\eta$ , in Table 3. Displacements in the y-direction are fluctuating at small values. This may include transverse displacements of the ground hitting the boundary at the bottom of the slope. Settlements (negative z-direction) show relatively good agreement between Models A and B.

For conventional scaling law in centrifuge modeling as listed in column (2) in Table 3, the scaling factor of displacement is identical with the scaling of length,  $\eta$ . For the GSL, the scaling factor of displacement is  $\mu^{1.5}\eta$ , which is  $\mu^{0.5}$  times larger than the scaling of length,  $\mu\eta$ . Fig. 20 shows the scaling factor for displacement versus the scaling factor for the length of the GSL used in each institute. In the conventional scaling

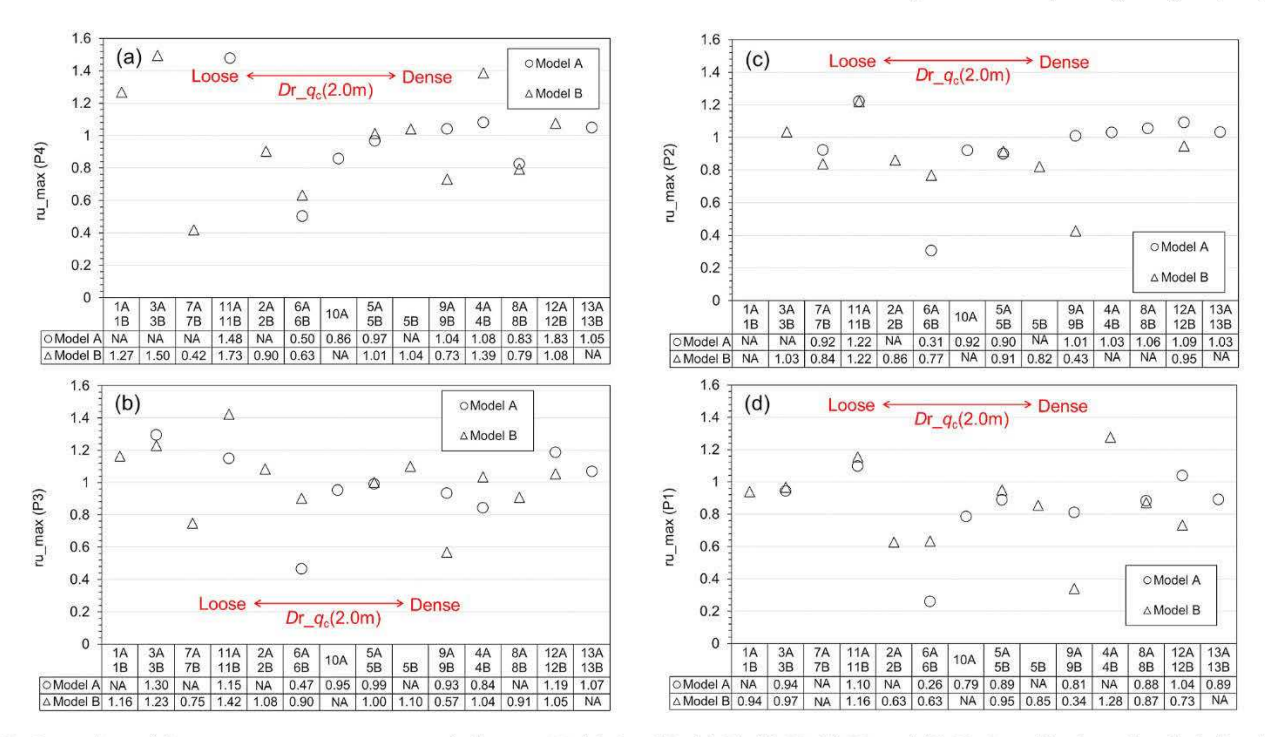


Fig. 15. Comparison of the excess pore water pressure ratio between Model A and B: (a) P4, (b) P3, (c) P2, and (d) P1. Sorted by the order of relative density.

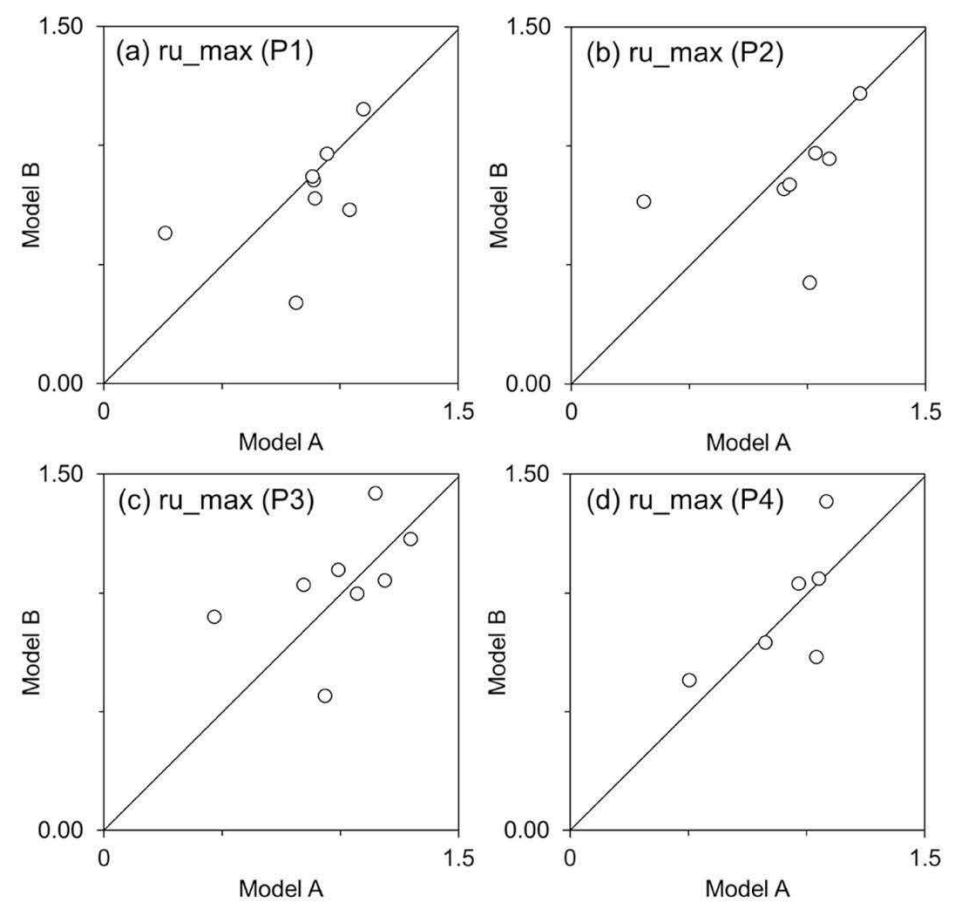


Fig. 16. Comparison of the maximum excess pore pressure ratio between Model A and B.

law of centrifuge modeling ( $\mu=1$ ), these dots line up on the straight line with 45°. The generalized scaling factor for displacement,  $\mu^{1.5}\eta$ , varies from 28.28 to 88.8 in the GSL with assigned values of scaling factor of

length for each institute. The generalized scaling factor for displacement,  $\mu^{1.5}\eta$ , may be kept within an acceptable range, close to the one-to-one line when the scaling factor of the virtual 1-g scaling,  $\mu$ , is in a range

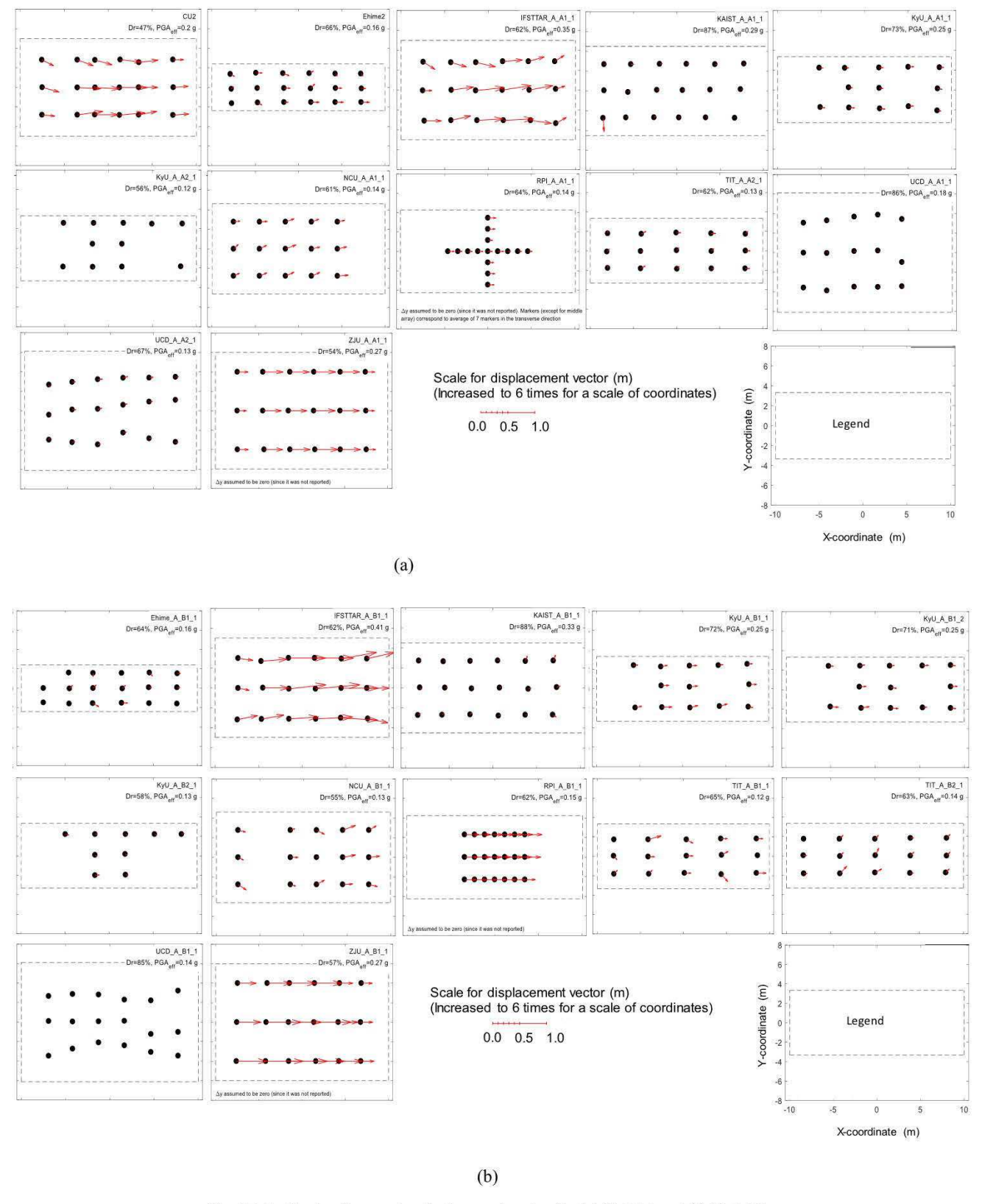


Fig. 17. Residual surface marker displacement vectors for (a) Model A and (b) Model B.

between 0.5 and 4.0 (Fig. 20). However, for the case of  $\mu=4$ , "KyU\_A\_B1\_2," deviation from the one-to-one line is relatively large. Thus, care should be taken in the planning phase of experiments with the GSL, especially when a larger virtual 1-g scaling factor (say  $\mu>2$ ) is used and/or larger ground displacements are expected. In such a case,

displacements in the prototype scale may be overestimated. However, as discussed in section 4.1, there may be some possibilities to reduce this gap with a modification of the virtual 1-g scaling law based on accurate measurements of ground stiffness with a CPT.

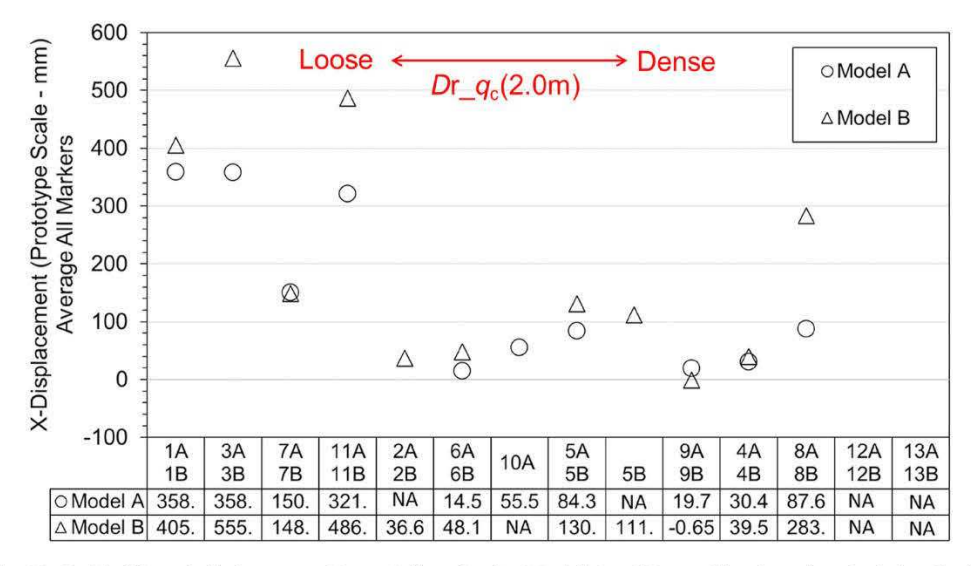


Fig. 18. Residual lateral displacements (Ave. of all markers) of Model A and B sorted by the order of relative density.

## 4.5. Correlation among $PGA_{eff}$ , $Dr_{qc}(2.0 \text{ m})$ , and surface displacements

Kutter et al. [15] found that, for lateral spreading, the residual surface displacements are primarily a function of the intensity of shaking and the relative density of the sand; a good correlation among these three variables was obtained, based on the results of UCD-2017. In this correlation, Kutter et al. [15] pointed out that, for a better agreement, the metrics that better represent the three variables are: " $U_{x2}$ " (average value of the residual displacement of the two central markers) for the displacement, the PGA<sub>eff</sub> for the intensity of shaking, and the  $Dr_{-}q_{c}(2.0 \text{ m})$  obtained from the CPT at the mid-depth of the model.

The shape of the surface in this correlation is based on the curves to estimate the maximum amount of generated shear strain, proposed by Yoshimine et al. [25], and the factors of safety for liquefaction, proposed by Idriss and Boulanger [26]. The regression equation is presented in Equation (4) [13].

$$U_{x2} = b_2 \left[ b_1 - \frac{\left( D_{r-} q_c(2.0m) - 0.125 \right)^{n_3} + 0.05}{1.3 PGA_{\text{eff}}} \right]^{n_1} \tag{4}$$

where  $b_1$ ,  $b_2$ ,  $n_1$ , and  $n_3$ , are coefficients obtained by regression analysis. Based on the results obtained in UCD-2017, and ASIA-2019, Vargas [19] updated the aforementioned correlation, to include the new findings, and establish a reliable and large centrifuge-models database. Fig. 21 shows a 3-D plot containing the whole experimental data from UCD-2017 and ASIA-2019. Aside from the existence of some tests out of the trend (that can be considered outliers and thus excluded), a significant improvement in the correlation can be observed because the  $R^2$  value increased from 0.75 to 0.90 (compared to the correlation developed only by considering UCD-2017 data).

Additionally for estimating the median value of the correlation, and as an attempt to estimate the variability in the tests, the upper and lower bounds for a 95% probability were estimated by assuming that the displacement values can be represented as a random variable that follows a Gaussian distribution. Table 6 shows the coefficients of Equation (4), and Fig. 22 shows the median trend and the upper/lower bounds for the updated correlation.

#### 5. Summary and conclusions

Following the model setup procedure established by LEAP-UCD-2017 [15], in LEAP-ASIA-2019, 10 international institutes conducted centrifuge model tests with various input conditions. In ASIA-2019, additionally to the conventional centrifuge model tests (Mode A),

model tests to validate the generalized scaling law (GSL) (Model B) were conducted. It was one of the first multi-institutional investigations into the validity of the generalized scaling law for saturated sandy sloping deposits with various initial conditions. The modeling of models technique was used to compare the dynamic responses of model ground of Model A and B. The results show that within a given range of input motions and initial density of the model ground, the generalized scaling factors for stress, acceleration, displacement, and time were validated within some tolerable ranges of errors using the scaling factors used in ASIA-2019 (virtual 1-g scaling factor of 0.5 <  $\mu$  < 4.0, centrifuge scaling factor of 11.1 <  $\eta$  < 71.6). Major results are summarized as follows:

- 1) In most test cases, a miniature CPT developed for UCD-2017 was used to measure the ground stiffness/strength. The CPT profiles tend to increase with depth in a range of 5–15 MPa in Models A and B. The tip resistance of Models A and B agree well at shallower depths but deviates as they go deeper. Although Models A and B achieved good agreements, Model B's tip resistance is systematically greater than Model A's. It may enable us to improve the 1-g scaling law based on accurate ground stiffness measurements.
- 2) Because the penetration resistance was highly influenced by the relative size of the container's width with a rod's diameter, a new power-type correlation was proposed between the tip resistance at the mid-depth, *q<sub>c</sub>*\_(2.0 m), and the dry density of the ground.
- 3) Dilatancy spikes induced by the deformation in the downstream direction are observed on shallow depth records in response to acceleration time histories. Records show that Models A and B have significant agreements in terms of waveforms for the tested range of input PGA and ground densities. Although the number of available measurements for Model B with the scaling factor of the virtual 1-g model being  $\mu < 1$ , is limited, overall waveforms and timing of spikes agree well with Model A.
- 4) Dilative spikes in the negative direction appear on the time histories of the excess pore-water pressure for models subjected to large input PGA and dense ground. A comparison of the maximum excess pore pressure ratio of P1 to P4 between Models A and B shows that, except for few, most of the values are close to the one-to-one relationship.
- 5) For the cases with a soft ground ( $\mathrm{Dr.q_c(2.0\ m)} < 55\%$ ) and large input  $\mathrm{PGA_{eff}}$  ( $\mathrm{PGA_{eff}} = 0.35$ ), residual ground surface deformation after the first destructive motion reached approximately 300–600 mm. The scaling factor for displacement versus the scaling factor for length used in each institute revealed that the generalized scaling factor for displacement,  $\mu^{1.5}\eta$ , varies from 28.3 to 88.8 with the scaling factor of the virtual 1-g scaling,  $\mu$ , ranging from 0.5 to 4.0. In this range of

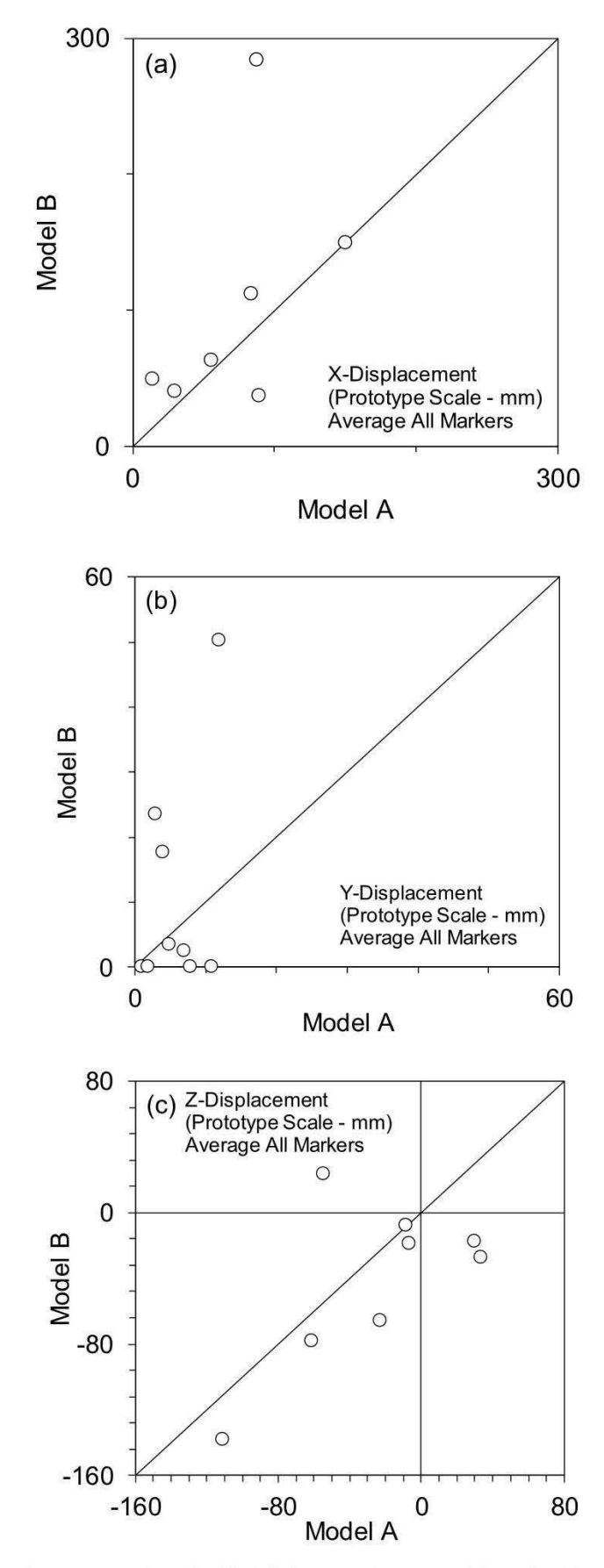


**Fig. 19.** Comparison of residual displacements between Model A and B: (a) x-, (b) y-, and (c) z-directions.

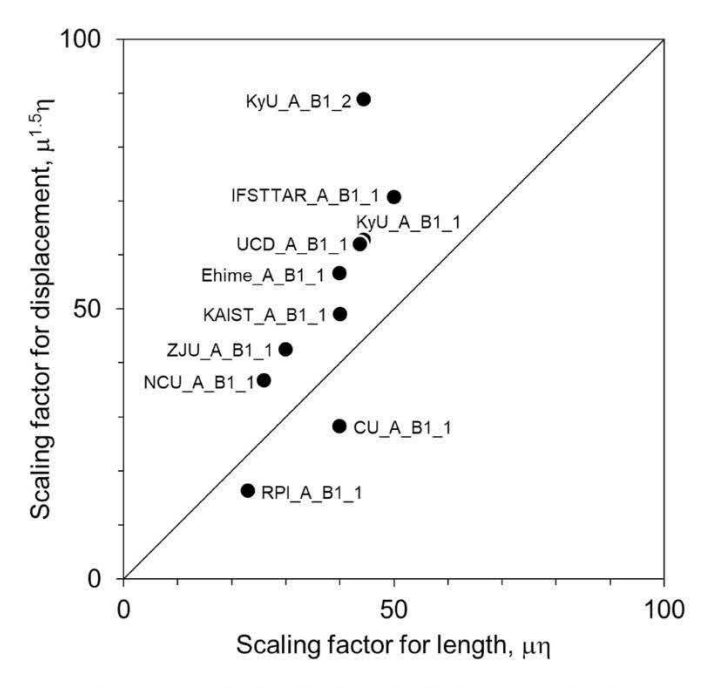


Fig. 20. Generalized scaling factor for displacement vs. length.

the virtual 1-g scaling factor,  $\mu$ , the generalized scaling factor for displacement,  $\mu^{1.5}\eta$ , may be kept within an acceptable range. However, caution should be taken during the planning phase of experiments with the GSL, especially when a larger virtual 1-g scaling factor (say  $\mu > 2$ ) is used or larger ground displacements are expected.

6) The correlation among  $\mathrm{Dr.}q_c(2.0~\mathrm{m})$ ,  $\mathrm{PGA_{eff}}$ , and  $\mathrm{U_{x2}}$  in the form of a three-dimensional (3-D) surface was updated by adding the new dataset obtained in LEAP-ASIA-2019. A significant improvement in the correlation was obtained using  $R^2=0.90$ . Additionally to estimating the correlation's median value, the upper and lower bounds for a 95% probability were estimated. These correlations can be used to effectively calibrate numerical methods.

It may be possible to estimate proper scaling factors of the 1-g scaling law using accurate measurements of ground stiffness taken with miniature CPT. This will be investigated further in the future.

## CRediT authorship contribution statement

Tetsuo Tobita: Conceptualization, Methodology, Validation, Investigation, Data curation, Writing - original draft, Supervision, Project administration, Funding acquisition. Kyohei Ueda: Validation, Investigation, Data curation, Supervision. Ruben R. Vargas: Validation, Investigation, Data curation, Visualization. Koji Ichii: Validation, Investigation, Data curation, Supervision. Mitsu Okamura: Validation, Investigation, Data curation, Supervision. Asri Nurani Sjafruddin: Validation, Investigation, Data curation. Jiro Takemura: Validation, Investigation, Data curation, Supervision. Lyu Hang: Validation, Investigation, Data curation. Ryosuke Uzuoka: Validation, Investigation, Data curation, Supervision. Susumu Iai: Conceptualization, Methodology, Supervision. Jad Boksmati: Validation, Investigation, Data curation. Alessandro Fusco: Validation, Investigation, Data curation. Samy Torres-Garcia: Validation, Investigation, Data curation. Stuart Haigh: Validation, Investigation, Data curation, Supervision, Project administration, Funding acquisition. Gopal Madabhushi: Validation, Investigation, Data curation, Supervision, Project administration, Funding acquisition. Majid Manzari: Conceptualization, Methodology, Supervision, Project administration, Funding acquisition. Sandra Escoffier: Validation, Investigation, Data curation, Supervision,

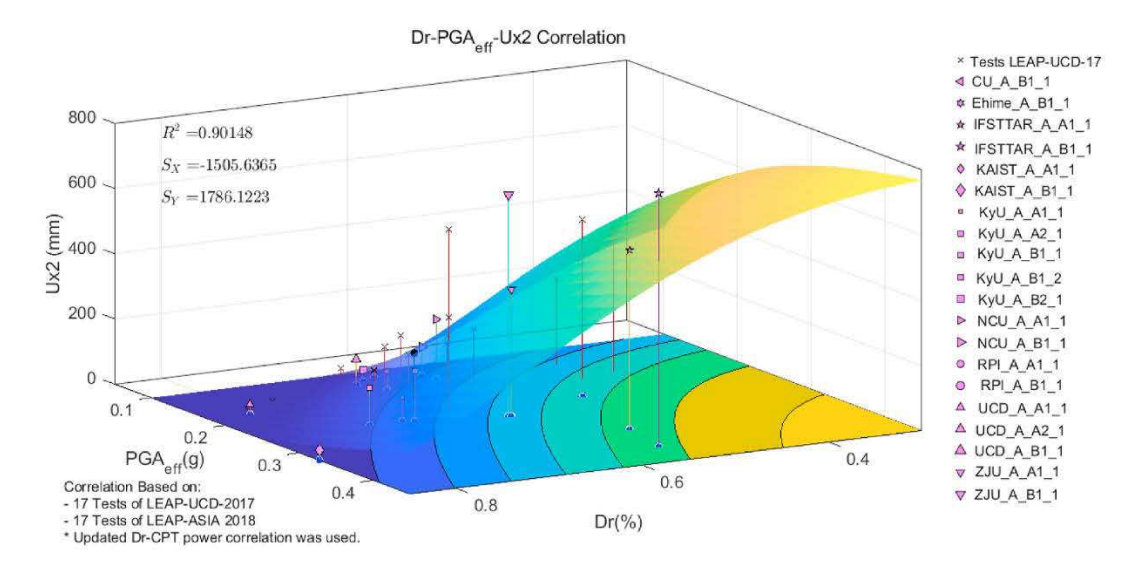
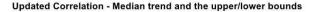
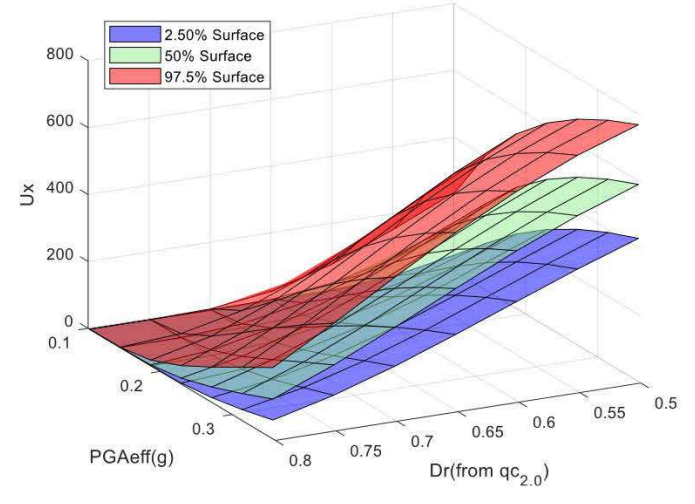


Fig. 21. Updated Correlation for Dr-PGA<sub>eff</sub>-U<sub>x</sub>. Correlation based on the 17 tests of LEAP-UCD-2017 & 17 tests of LEAP-ASIA 2019 (Model A & B) [21].

**Table 6**Coefficients for the updated correlation – Median values, Lower Bounds, and Upper Bounds for a 95% probability [19].

Coefficient	Lower bound	Median	Upper bound
$b_1$	1.678	1.756	1.834
$b_2$	100	100	100
$n_1$	4	4	4
$n_3$	2.855	3.245	3.635





**Fig. 22.** Updated correlation, comparison between the median trend (50% Surface) and the Upper (97.5% Surface)/Lower (2.5%) Bounds for a 95% probability [21].

Project administration, Funding acquisition. Zheng Li: Validation, Investigation, Data curation. Dong Soo Kim: Validation, Investigation, Data curation, Project administration, Funding acquisition. Satish Manandhar: Validation, Investigation, Data curation. Wen-Yi Hung: Validation, Investigation, Data curation, Project administration, Funding acquisition. Jun-Xue Huang: Validation, Investigation, Data curation. Truong-Nhat-Phuong Pham: Validation, Investigation, Data curation. Mourad Zeghal: Conceptualization, Methodology, Supervision, Project administration, Funding acquisition. Tarek Abdoun: Validation, Investigation, Data curation, Supervision. Evangelia Korre:

Validation, Investigation, Data curation. Bruce L. Kutter: Conceptualization, Methodology, Supervision, Project administration, Funding acquisition. Trevor J. Carey: Validation, Investigation, Data curation. Nicholas Stone: Validation, Investigation, Data curation. Yan-Guo Zhou: Validation, Investigation, Data curation, Supervision, Project administration, Funding acquisition. Kai Liu: Validation, Investigation, Data curation. Qiang Ma: Validation, Investigation, Data curation.

#### Declaration of competing interest

The authors declare that they have no known competing financial interests or personal relationships that could have appeared to influence the work reported in this paper.

#### Acknowledgments

The experimental work on LEAP-ASIA-2019 was supported by different funds depending mainly on the location of the work. The work at Kyoto U., Ehime U., Tokyo Institute of Technology and Kansai U., Japan, was supported by JSPS KAKENHI Grant Number 26282103 and 17H00846. The work by the US PI's (Manzari, Kutter, and Zeghal) is funded by National Science Foundation grants: CMMI 1635524, CMMI 1635307 and CMMI 1635040. The work at KAIST, Korea, was part of a project titled "Development of performance-based seismic design," funded by the Ministry of Oceans and Fisheries, Korea. The work at Zhejiang U., China, was supported by NSF (Nos. 51778573, 51978613, 51988101) and the 111 Project (No. B18047). The work at National Central University, Taiwan, was supported by MOST: 106-2628-E-008-004-MY3.

## References

- [1] Arulanandan K, Scott RF. Verification of numerical procedures for the analysis of soil liquefaction problems, proceedings of the international conference on the verification of numerical procedures for the analysis of soil liquefaction problems1 and 2. Rotterdam. Netherland: A. A. Balkema: 1994.
- [2] Iai S, Matsunaga Y, Kameoka T. Strain space plasticity model for cyclic mobility. Soils Found 1992;37(2):1–15.
- [3] Iai S, Ueda K, Tobita T, Ozutsumi O. Finite strain formulation of a strain space multiple mechanism model for granular materials. Int J Numer Anal Methods GeoMech 2013;37(9):1189-212.
- [4] Oka F, Yashima A, Tateishi Y, Taguchi Y, Yamashita S. A cyclic elasto-plastic constitutive model for sand considering a plastic-strain dependence of the shear modulus. Geotechnique 1999;49(5):661–80.
- [5] Boulanger RW, Ziotopoulou K. PM4Sand (version 3): a sand plasticity model for earthquake engineering applications. In: Report No. UCD/CGM-15/01 center for geotechnical modeling. California: Department of Civil and Environmental Engineering, University of California Davis; 2015.

- [6] Asaoka A, Noda T. All soils all states all round geo-analysis integration, international workshop on constitutive modelling - development, implementation, evaluation, and application, Hong Kong, China. 2007. p. 11–27.
- [7] Cundall PA, Strack ODL. A discrete numerical model for granular assemblies. Geotechnique 1979;29(1):47–65.
- [8] Lucy LB. A numerical approach to the testing of the fission hypothesis. Astron J 1977;82:1013-24.
- [9] Monaghan JJ. Smoothed particle hydrodynamics. Annu Rev Astron Astrophys 1992;30:543–74.
- [10] Koshizuka S, Oka Y. Moving-particle semi-implicit method for fragmentation of incompressible fluid. Nucl Sci Eng 1996;123(3):421–34.
- [11] Manzari MT, Kutter BL, Zeghal M, Iai S, Tobita T, Madabhushi G, Haigh SK, Mejia L, Gutierrez DA, Armstrong RJ, Sharp MK, Chen YM, Zhou YG, LEAP projects: concept and challenges, geotechnics for catastrophic flooding events. CRC Press; 2015. p. 109–16.
- [12] Manzari TM, Ghoraiby M, Kutter BL, Zeghal M, Abdoun T, Arduino P, Armstrong RJ, Beaty M, Carey T, Chen Y-M, Ghofrani A, Gutierrez D, Goswami N, Haigh SK, Hung W-Y, Iai S, Kokkali P, Lee C-J, Madabhushi G, Mejia L, Sharp M, Tobita T, Ueda K, Zhou Y-G, Ziotopoulou K. Liquefaction experiment and analysis projects (LEAP): summary of observations from the planning phase, Soil Dynamics and Earthquake Engineering, LEAP2015 Special volume, Ed. Manzari, Kutter and Zeghal, 113; 2018. p. 714–43. https://doi.org/10.1016/j.soildyn.2017.05.015.
- [13] Kutter B, Carey T, Hashimoto T, Zeghal M, Abdoun T, Kokalli P, Madabhushi G, Haigh S, Hung W-Y, Lee C-J, Iai S, Tobita T, Zhou YG, Chen Y, Manzari MT. LEAP-GWU-2015 experiment specifications, results, and comparisons. Soil Dynam Earthq Eng 2018;113:616–28. https://doi.org/10.1016/j.soildyn.2017.05.018.
- [14] Kutter BL, Carey TJ, Stone N, Bonab MH, Manzari MT, Zeghal M, Escoffier S, Haigh SK, Madabhushi G, Hung W-Y, Kim D-S, Kim NR, Okamura M, Tobita T, Ueda K, Zhou Y-G. LEAP-UCD-2017 V. 1.01 model specifications. In: Kutter B, Manzari MT, Zeghal M, editors. Model tests and numerical simulations of liquefaction and lateral spreading. Springer OPEN; 2020. p. 3–29. https://doi.org/10.1007/978-3-030-22818-7\_1.
- [15] Kutter BL, Carey TJ, Stone N, Zheng BL, Gavras A, Manzari MT, Zeghal M, Abdoun T, Korre E, Escoffier S, Haigh SK, Madabhushi G, Madabhushi S, Hung W-Y, Liao T-W, Kim D-S, Kim S-N, Ha J-G, Kim NR, Okamura M, Sjafruddin AN,

- Tobita T, Ueda K, Vargas R, Zhou Y-G, Liu K. LEAP-UCD-2017 comparison of centrifuge test results. In: Kutter B, Manzari MT, Zeghal M, editors. Model tests and numerical simulations of liquefaction and lateral spreading. Springer OPEN; 2020. p. 69–103. https://doi.org/10.1007/978-3-030-22818-7\_4.
- [16] Iai S, Tobita T, Nakahara T. Generalized scaling relations for dynamic centrifuge tests. Geotechnique 2005;55(5):355-62.
- [17] Tokimatsu K, Suzuki H, Tabata K, Sato M. Three dimensional shaking table tests on soil-pile-structure models using E-Defense facility, 4th International Conference on Earthquake Engineering, June 25-28, Thessaloniki, Greece. 2007.
- [18] Iai S. Similitude for shaking table tests on soil-structure-fluid model in 1g gravitational field. Soils Found 1989;29(1):105–18.
- [19] Carey T, Gavras A, Kutter BL. Chapter 6 comparison of LEAP-UCD-2017 CPT results. In: Kutter B, Manzari MT, Zeghal M, editors. Model tests and numerical simulations of liquefaction and lateral spreading: LEAP-UCD-2017. Springer OPEN; 2020. p. 117-29. https://doi.org/10.1007/978-3-030-22818-7\_6.
- [20] Bolton MD, Gui MW, Garnier J, Corte JF, Bagge G, Laue J, Renzi R. Centrifuge cone penetration tests in sand. Geotechnique 1999;49(4):543–52.
- [21] Vargas R. Validation of numerical predictions of lateral spreading based on "hollow-cylinder torsional shear tests" and "a large centrifuge-models database", Master Thesis submitted to Department of Civil and Earth Reources Engineering. Kyoto University; 2020.
- [22] Carey TJ, Stone N, Kutter BL. Chapter 2 Grain size analysis and maximum and minimum dry density of Ottawa F-65 sand for LEAP-UCD-2017 B. In: Kutter M T Manzari, Zeghal M, editors. Model tests and numerical simulations of liquefaction and lateral spreading. Springer OPEN; 2020. p. 31–44. https://doi.org/10.1007/ 978-3-030-22818-7 2.
- [23] Adamidis O, Madabhushi G. Use of viscous pore fluids in dynamic centrifuge modeling. Int J Phys Model Geotech 2015;15(3):141–9.
- [24] Stewart DP, Chen Y-R, Kutter BL. Experience with the use of Methylcellulose as a viscous pore fluid in centrifuge models. Geotech Test J 1998;21(4):365-9.
- [25] Yoshimine M, Nishizaki H, Amano K, Hosono Y. Flow deformation of liquefied sand under constant shear load and its application to analysis of flow slide in infinite slope. Soil Dynam Earthq Eng 2006;26:253-64.
- [26] Idriss IM, Boulanger RW. Soil liquefaction during earthquakes. Oakland, California, USA.: Earthquake Engineering Research Institute (EERI); 2008. MNO-12.